



Constraints on Dark Photon Production from Dilepton Sources at SIS Experiment

Abschlussarbeit zur Erlangung des akademischen Grades
Bachelor of Science (B.Sc.) in Physik

an der Johann Wolfgang Goethe-Universität Frankfurt am Main,
angefertigt am Institut für Theoretische Physik des Fachbereichs Physik,
vorgelegt von

Ida Marie Schmidt

geboren am 22. Januar 1999 in Marburg/Wehrda, Deutschland

Erstgutachterin: Prof. Dr. Elena Bratkovskaya

Zweitgutachter: Prof. Dr. Marcus Bleicher

Abgabe der Arbeit am 18. Januar 2021

Erklärung

Ich versichere hiermit, dass ich die vorliegende Arbeit selbstständig verfasst und keine anderen als die im Literaturverzeichnis angegebenen Quellen benutzt habe. Ich habe die Regeln der guten wissenschaftlichen Praxis eingehalten.

Alle Stellen, die wörtlich oder sinngemäß aus veröffentlichten oder noch nicht veröffentlichten Quellen entnommen sind, sind als solche kenntlich gemacht.

Die Zeichnungen oder Abbildungen in dieser Arbeit sind von mir erstellt worden oder mit einem entsprechenden Quellennachweis versehen.

Diese Arbeit ist in gleicher oder ähnlicher Form noch bei keiner anderen Prüfungsbehörde eingereicht worden.

Ort, Datum

Ida Schmidt

Acknowledgements

First and foremost, I want to thank Prof. Elena Bratkovskaya for supervising my thesis and for her outstanding patience and explanations during this time.

Also, I thank Olga Soloveva and Ilia Grishmanovskii for answering my questions regarding the cluster.

Special thanks go to Jan Röder for supporting me at any time I had to sort my mind and for his sharp criticism and Hella Schmidt for proofreading my thesis and always encouraging me.

Contents

List of Figures	6
List of Abbreviations	9
1 Abstract	10
2 Motivation	11
3 Short Introduction to Dark Matter	13
3.1 Evidence for Dark Matter	13
3.2 WIMPs and Mediator Particles	14
3.3 Experimental Measurement Approaches	15
3.3.1 Direct Measurement	15
3.3.2 Indirect Measurement	16
3.3.3 Astrophysical Probes	16
3.3.4 Particle Colliders	16
3.4 Structure of the Universe	17
4 Extension of the Standard Model: Dark Sector, Portals, and A' gauge bosons	18
4.1 The Standard Model	18
4.2 Extensions beyond the Standard Model	19
4.3 Portal Interactions	19
4.4 Dark Photons	20
5 Theoretical Approach	21
5.1 PHSD	21
5.2 Studies of Au+Au collisions	23
5.2.1 Rapidity and Transverse Momenta	23
5.2.2 Centrality and Impact Parameter	25
5.3 Dilepton Sources	29
5.3.1 General	29
5.3.2 Direct Decay	30
5.3.3 Dalitz Decay	30
5.4 Dilepton Spectra	32

6	Experimental Dilepton Spectra	36
6.1	The HADES experiment	36
6.2	Dilepton Sepctra by HADES	36
6.3	Measuring Techniques for invisible particles	38
6.3.1	Excess in Dilepton Spectra	39
7	Finding a Dark Photon	40
7.1	Interaction	40
7.1.1	The role of the Mixing Parameter	42
7.2	Theoretical Calculations	43
7.2.1	Implementing U-Boson contributions in the PHSD	43
8	The Goal: finding an upper limit for ϵ^2	49
8.1	Resulting ϵ^2	53
9	Conclusions	55

List of Figures

1	Left: observed rotation curve in comparison with the expectation. The velocity increases significantly faster and stays stable instead of dropping [5]. Right: Picture of Bullet Cluster. The two galaxy clusters on the left and right of the collision zone passed each other, while the gas stayed in the collision zone. The figure is taken from [6].	13
2	Interaction of an SM particle with a DM particle via an unknown mediator [9].	14
3	Interaction candidates and experimental methods. The lines connect the possible interaction partners with the experiments in which they can be found [10].	15
4	Presence of DM in the universe. Figure is taken from [13].	17
5	Current version of the SM. Figure is taken from [14].	18
6	Different options for portals. Their mediator particles are written in the middle and their gauge operators on the right. Table is taken from [3] . . .	20
7	Left: Rapidity distributions for protons (p) and π^\pm for 1.23 A GeV Au+Au collisions at $b = 2.25$ fm. Right: Transverse momentum distributions for protons and π^\pm for 1.23 A GeV Au+Au collisions at $b = 2.25$ fm.	24
8	Graphical description of the impact parameter. The larger b , the less central the collision and the less participants contribute to the collision. Figure is taken from [23].	25
9	Left: Number of participants in dependence on centrality b in Au+Au collisions at 1.23 A GeV. Right: Multiplicities for protons and π^\pm in Au+Au collisions at 1.23 A GeV vs N_{part}	26
10	Rapidity distributions for protons (p) and π^\pm for 1.25 A GeV Au+Au collisions at $b = 10.0$ fm. Right: Transverse momentum distributions for protons and π^\pm for 1.25 A GeV Au+Au collisions at $b = 10.0$ fm.	27
11	Left: Rapidity distribution for protons p and π^\pm for 1.23 A GeV Au+Au collisions for $b = [0.25, 14.5]$ fm. Right: Transverse momentum distributions for protons and π^\pm for 1.23 A GeV Au+Au collisions for $b = [0.25, 14.5]$ fm. b is increased with a constant step of 0.25 fm.	28
12	Direct decay of a vector meson into a dielectron pair via a virtual photon γ^* . 30	
13	Dalitz decay of a pseudoscalar meson (π^0 or η) via a virtual photon γ^* into a dielectron pair while emitting another photon γ	31
14	Dalitz decay of a Δ resonance via a virtual photon γ^* into a dielectron pair. 32	

15	Differential cross-section $d\sigma/dM$ for e^+e^- production in p+p reactions at 3.5 GeV beam energy. The theoretical calculation from PHSD is compared to HADES data [26]. The different color lines display individual channels in the transport calculation (see legend).	33
16	Differential cross-section $d\sigma/dM$ for e^+e^- production in p+Nb reactions at 3.5 GeV beam energy. The theoretical calculation from PHSD is compared to HADES data [24, 25]. The different color lines display individual channels in the transport calculation (see legend).	34
17	Mass differential dilepton spectra dN/dM normalized to π^0 multiplicity for Ar+KCl reactions at 1.76 A GeV and $b = 0.5 - 6.0$ fm centrality. The theoretical calculation from PHSD is compared to HADES data [27]. The different color lines display individual channels in the transport calculation (see legend).	35
18	(a) Dielectron mass resolution (FWHM) as a function of the e^+e^- invariant mass obtained from a Monte-Carlo simulation. (b) Inclusive dilepton spectra from HADES experiment for Ar+KCl at 1.76 A GeV, p+p, and p+Nb at 3.5 GeV with statistical error bars. The plot is taken from [29].	37
19	Extracted 90% confidence level (Confidence Level) upper limits for a narrow $U \rightarrow e^+e^-$ signal found by HADES for p+p (left), p+Nb (middle) and Ar+KCl (right). Pink line: computed experimental sensitivity. The error bands are printed in yellow (1σ) and blue (2σ). The expected excess in the number of counts is plotted for a 90% CL against the U-Boson mass M_U . The plot is taken from [29].	39
20	Dalitz decay of a vector meson (π^0 or η) via a U-Boson U into a dielectron pair while emitting another photon γ	40
21	Dalitz decay of a Δ resonance via a U-Boson U into a dielectron pair.	41
22	HADES ϵ^2 from Ar+KCl, p+p, and p+Nb spectra in dependence on the U-Boson mass M_U . Figure is taken from [29].	42
23	Comparison of combined ϵ^2 results with other experiments. Figure is taken from [29].	43
24	Branching ratio vs M_U [29].	44
25	Decay widths Γ of π^0 and η to $U+\gamma$ for $\epsilon^2 = 1$	46
26	Decay widths of Δ resonances to $N+U$ for $M_\Delta = 1.23$ GeV and $M_\Delta = 2$ GeV at $\epsilon^2 = 1$	47
27	Decay widths of π^0 and η to $U+\gamma$	48
28	Decay widths of Δ resonances to $U+N$ at $M_\Delta = 1.23$ GeV and $M_\Delta = 2$ GeV.	48

29	Differential cross-section $d\sigma/dM$ for e^+e^- production in p+p reactions at 3.5 GeV beam energy. The theoretical calculation from PHSD is compared to HADES data [26]. The different color lines display individual channels in the transport calculation (see legend). Included are the contributions from potential $U \rightarrow e^+e^-$ are shown as red triangles.	50
30	Differential cross-section $d\sigma/dM$ for e^+e^- production in p+Nb reactions at 3.5 GeV beam energy. The theoretical calculation from PHSD is compared to HADES data [24, 25]. The different color lines display individual channels in the transport calculation (see legend). Included are the contributions from potential $U \rightarrow e^+e^-$ are shown as red triangles.	51
31	Mass differential dilepton spectra dN/dM normalized to π^0 multiplicity for Ar+KCl reactions at 1.76 A GeV and $b = 0.5 - 6.0$ fm centrality. The theoretical calculation from PHSD is compared to HADES data [27]. The different color lines display individual channels in the transport calculation (see legend). Included are the contributions from potential $U \rightarrow e^+e^-$ are shown as red triangles.	52
32	Theoretical ϵ^2 extracted from dilepton spectra in comparison with experimental HADES ϵ^2	53
33	Constraints on ϵ^2 from other experiments. Figure is taken from [3].	54

Abbreviations

DM Dark Matter

DP Dark Photon

DQPM Dynamical Quasi Particle Model

HADES High Acceptance Dielectron Spectrometer

HSD Hadron String Dynamics

PHSD Parton Hadron String Dynamics

QGP Quark Gluon Plasma

SIS Schwerionensynchrotron

SM Standard Model

WIMP Weakly Interacting Massive Particle

1 Abstract

The nature of the second-most present substance in our universe, Dark Matter, is almost completely unknown from today's perspective. Researching its gravitational properties and impact on the universe's formation has been a task for astrophysicists over the last decades. Over the years, more research methods were developed independent of astrophysical measurements.

At the HADES experiment in Darmstadt, the search for Dark Matter is done using decays in dilepton spectra that may include Dark Photons. These unknown particles are supposed to mediate the interaction between Dark Matter and ordinary matter and should therefore couple to ordinary matter. An experimentally found upper limit for the coupling constant of Dark Photons to ordinary matter was obtained by HADES. The goal of this thesis is to find an according theoretical upper limit for the coupling constant using the PHSD approach for the calculation of dilepton spectra and Dark Photon contributions.

2 Motivation

The search for Dark Matter (DM) has been going on for decades. Modern measuring techniques and calculation methods provide new opportunities to search for WIMPs (Weakly Interacting Massive Particles) or their mediator particles. Reaching from astrophysical research over strategies aiming to detect Dark Matter from outer space to experiments at particle colliders, the topic covers a vast research field.

An exciting and promising approach to finding signals caused by Dark Matter particles offers the decay of a particle via dark mediator particles into ordinary particles. By measuring the decay products, it is possible not only to find a proof for Dark Matter but also learn about its properties, the mass of the mediator, and its couplings to ordinary standard model (SM) matter. One of these mediator particles is the Dark Photon (DP), which will be the main interest of this thesis. It acts as an exchange boson in DM interactions with SM matter and can thereby be detected indirectly through an excess in the measured decay products.

Particle colliders have the opportunity to measure these decays. They are not only completely independent of any astrophysical observation, but they also have the ability to search very specifically for Dark Photons. They are assumed to occur in dilepton decays. The HADES experiment at GSI in Darmstadt measures dilepton spectra by using beams from the SIS ring accelerator. The search for Dark Photons at HADES provides exciting possibilities for new observations on Dark Matter. Experiments were done to obtain an experimental upper limit for the coupling of Dark Photons to SM matter.

This thesis aims to calculate dilepton spectra at mass and energy ranges as they are measured by the HADES experiment and implement theoretical contributions caused by Dark Photon decays. In comparison to the HADES data and results, theoretical predictions regarding the decays of Dark Photons and their coupling constants will be made.

The thesis is structured as follows. Chapter 3 presents a general introduction to Dark Matter, including different approaches to research it. The ideas of WIMPs and mediator particles will be explained as a basis for the following models. Chapter 4 explains to Dark Photons. They are new, unknown particles that are not included in our SM which need a theoretical description first. For this purpose, a short overview of the SM is given, followed by possible extensions to include new particles. This leads to the Dark Sector and Portal interactions, providing an accurate theoretical description of a Dark Photon.

Subsequently, the theoretical and experimental backgrounds used for this study are explained in chapters 5 and 6. They describe the general basics of heavy-ion collisions and dilepton sources. The obtained SM matter spectra, which are the basics for any further

calculations, are shown. On this basis, the analysis of Dark Photon contributions is done in chapter 7. The resulting contributions are presented here as well. As a final result, the theoretically obtained upper limit for the coupling constant of a Dark Photon versus its mass is presented in chapter 8.

3 Short Introduction to Dark Matter

3.1 Evidence for Dark Matter

The first observations on Dark Matter go back to the 1930s when Fritz Zwicky observed the galaxies' movements in the *Coma Cluster* [1]. This galaxy cluster contains over 1000 galaxies with each a different single velocity. Due to the galaxies' motions, this cluster can not be held together by purely the gravity of the observed, visible matter. According to his observations, Zwicky proposed some extra matter within the galaxies, which he called *Dark Matter* [2]. The name of a new research field was set.

Over the following decades, ongoing research on astrophysical effects took place [3]. The most popular is Vera Rubin's research on the rotation velocity of spiral galaxies [4]. The rotation velocities of the outer parts of a galaxy were way too large for a stable galaxy.

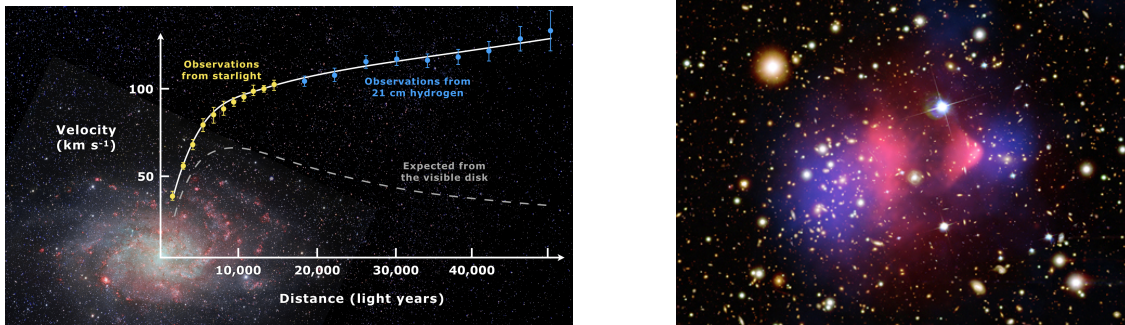


Figure 1: Left: observed rotation curve in comparison with the expectation. The velocity increases significantly faster and stays stable instead of dropping [5]. Right: Picture of Bullet Cluster. The two galaxy clusters on the left and right of the collision zone passed each other, while the gas stayed in the collision zone. The figure is taken from [6].

Further observation and data collection gave the final proof: there is more to these observations than we can describe with our current models.

The most impressive evidence for Dark Matter was found in the Bullet Cluster (fig. 1). Two galaxy clusters, consisting of galaxies and interstellar nebula, collided. The galaxies passed each other due to their large distances without any collision. The gas distributed in between makes a surprisingly large amount of matter. It remained in the collision zone. Observations show that still the major part of the mass remained in the clusters. This effect can only be explained by additional matter that exists only within the galaxies! Any other hypothesis to describe only the gravitational effects fails here [7].

The most likely approach is to presume additional matter in the galaxies, as initially proposed by Zwicky. For this matter, MACHOs (Massive Astrophysical Compact Halo

Objects) that do not interact with light and consist of ordinary SM matter were ruled out as candidates - they make less than 1% of a galaxy's matter [8].

Instead, the additional matter must be a new kind of matter beyond our known Standard Model. Its properties are completely unknown except for its gravitational impact on galaxies. To find out more about this Dark Matter, researchers found several experimental research methods. For this, it is assumed that DM particles are so-called WIMPs: Weakly Interacting Massive Particles.

3.2 WIMPs and Mediator Particles

As mentioned before, WIMPs are believed to be very heavy particles with gravitational impact and to interact weakly with SM particles. WIMPs themselves are then the unknown DM particles [9]. The WIMP's interaction with any kind of matter (self-interactions and SM couplings) takes place via *mediator particles*. The couplings of mediators are described closer by *portals* [3], which will be explained in chapter 4.3. For now, it is essential to mention that mediator particles can as well be unknown DM particles and will need further research themselves - Dark Photons are some of them.

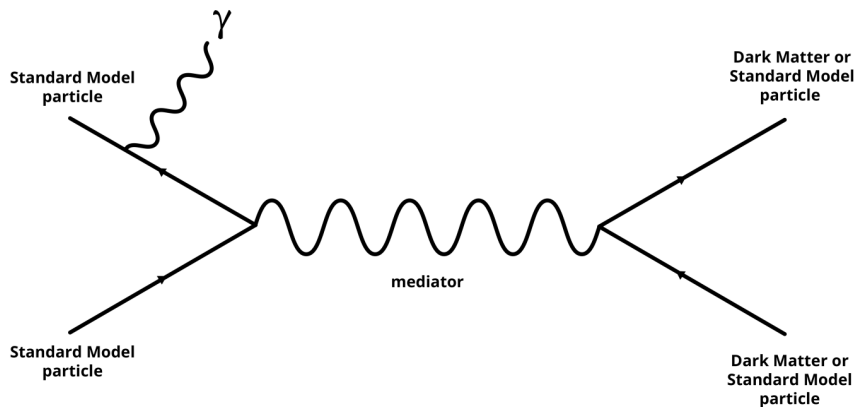


Figure 2: Interaction of an SM particle with a DM particle via an unknown mediator [9].

The decay products or scattering properties of WIMPs and mediators are used to find Dark Matter experimentally. A short overview of the different approaches is given in the next chapter.

3.3 Experimental Measurement Approaches

The interaction of WIMPs can take place with four categories of particles [10]. These categories and the according measuring approaches are illustrated in fig. 3.

Research on the interactions between known matter such as nuclear matter, leptons, and photons is carried out by experiments on Earth that use direct or indirect measurement techniques. Particle colliders focus on the interactions with leptons and nuclear matter. Astrophysical probes are somewhat different - they do not aim to find DM particles directly or find out about the specifics of interactions, but observe the universe's formation and its behavior, as well as possible effects of DM self-interactions.

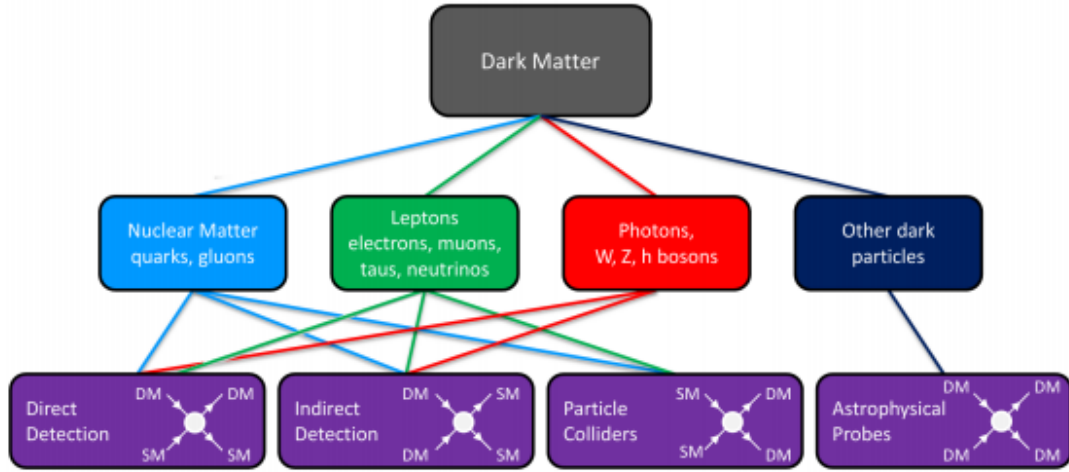


Figure 3: Interaction candidates and experimental methods. The lines connect the possible interaction partners with the experiments in which they can be found [10].

3.3.1 Direct Measurement

Dark Matter particles are assumed to be present in galaxies, including the Milky Way. Therefore, they should hit the Earth eventually. The scattering on the nuclei of a detector material can be used to produce detectable signals.

The Dark Matter density is assumed to be locally homogeneous and moves in one direction (also locally - when talking about the whole galaxy, the movement differs) [11]. According to the Earth's circular motion around the sun, the Earth moves along the Dark Matter velocity at one time of the year and against it half a year later [12]. Considering this, depending on the time of the year, more or less DM particles should be measured. If

particles and the predicted dependence on the time of the year are measured, we also learn about the DM movement in the Milky Way [10].

3.3.2 Indirect Measurement

The detection of decay products of Dark Matter particles in space is called indirect detection. It assumes that either a pair of interacting Dark Matter particles in outer space annihilate and thereby create decay products in a particular energy range or that DM particles are captured by the sun. Once this happened, they sink into the sun and gain energy. At some point, they hit another SM particle and interact with it, causing new high-energy decay products (these could be neutrinos or antimatter, for example). The decay products leave the sun undisturbed and hit the Earth eventually, where detectors can find them [10].

3.3.3 Astrophysical Probes

Astrophysical probes are different from other experiments because they do not look for the particle nature of Dark Matter directly. Instead, they aim to give insights on the temperature or self-interaction of Dark Matter by studying the formation of the universe (such as galaxy clusters and rotation curves). Astrophysicists also search for dark sub-halos in the halos of galaxies to sufficiently explain the gravitational observations [10].

3.3.4 Particle Colliders

An exciting measuring approach is the search for Dark Matter in particle colliders. This has the great advantage of being independent of any astrophysical measurement, making it unique and very promising.

The measuring approaches base on the same assumptions as other approaches - the interaction of WIMPs with SM matter and the existence of new mediators. By detecting possible decay products at given beam energies, people can gather knowledge on the mediators. If WIMPs are produced in a reaction, they can be tracked by the transverse momentum they carry away. Both techniques are further explained in chapter 6.3.

3.4 Structure of the Universe

According to various astrophysical observations, 24% of the universe's matter is made of Dark Matter [13]. This is more than five times the amount of our ordinary matter, making only about 4.6%. The remaining 71.4% go to Dark Energy, which is thought to be homogeneously distributed over the universe, unlike Dark Matter, which is present only within galaxies - it is a whole different topic.

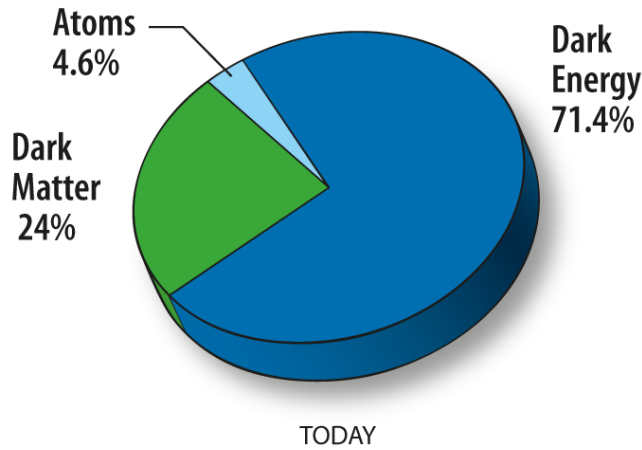


Figure 4: Presence of DM in the universe. Figure is taken from [13].

Over the last century, it has become evident that we only know the smallest part of our universe. To gain knowledge on the new sort of matter and understand and include it in our current models, various options have come up.

4 Extension of the Standard Model: Dark Sector, Portals, and A' gauge bosons

How can WIMPs and their mediator particles be included in the SM? This is an important question to ask since we want to fully describe the properties interactions of Dark Matter, also with SM particles. Therefore, they have to be a part of some new version of the SM.

4.1 The Standard Model

The SM of particles was established in the last century to describe the interactions of two different sorts of particles: Spin-1/2 fermions and spin-1 gauge bosons. Also included is the spin-0 Higgs boson. The SM can explain a large part of our known world but is certainly incomplete.

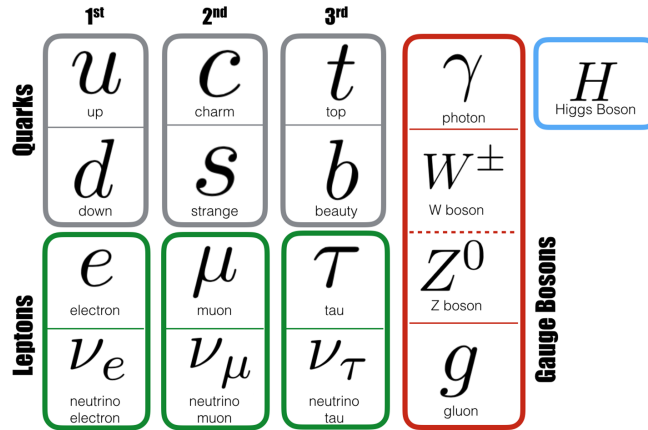


Figure 5: Current version of the SM. Figure is taken from [14].

The ordinary SM matter that surrounds us can be separated into two main categories, leptons and quarks. Both groups consist of six particles, paired in generations. The lightest and most stable particles are the first generation, the heaviest and least stable the third. Additionally, there are four fundamental forces: gravitational, electromagnetic, strong, and weak force. Electromagnetic, strong, and weak interactions result from the exchange of known gauge bosons that are as well included in the SM: photons, gluons, and W^\pm and Z^0 exchange bosons. Gravity, however, is lacking such a gauge boson up to nowadays knowledge. The existence of a possible graviton to describe the interaction has not been proven.

Next gravity, the SM does also not incorporate DM particles and their interactions and

fails to explain the excess of matter against anti-matter. Adaptions and extensions of the SM are discussed for many reasons and in many different ways, including extensions for DM. The following chapters will give some insights on the extensions for DM.

4.2 Extensions beyond the Standard Model

As already said in the last chapter, Dark Matter and Dark Energy make about 80% of the universe's whole matter. So the largest part of the existing matter is an unknown substance whose interactions and constituents differ a lot from known SM matter. The absence of evidence for WIMPs in direct detection methods or at particle colliders motivates a theory beyond the SM. Introducing a new sector of the SM with a new force through which Dark Matter can interact with SM matter, but couples only indirectly to it makes a suitable approach. *Dark Sectors* provide a relatively simple approach to extending the SM and, therefore, sensibly describing Dark Matter [3]. The main properties of DM are its lack of electromagnetic and strong interactions and its large occurrence in the universe. A Dark Sector can explain those interactions, and DM occurrence in the universe can be explained by thermal freeze-in and freeze-out. This makes it a very natural approach to describe DM. The most significant focus when searching for Dark Sectors is the most accessible portal, which is gauge kinematic mixing [3].

The Dark Sector could include all Dark Matter particles and their interactions. This is an essential feature since there is about five times more Dark Matter in the universe than SM matter - and the SM matter is already extremely diverse!

The Dark Sector will then contain all dark particles. Their interactions with SM matter will be described using so-called *portals*, a fundamental concept for my thesis, and will therefore be described in the following chapter in detail.

4.3 Portal Interactions

Portals are a way to describe the interactions of DM particles with SM particles. As already mentioned several times, the interaction takes place via a mediator particle. Portals represent these mediators and their coupling to SM matter.

There are different options to choose a portal. The choice depends on the mediator's spin and parity - according to this, the portal is named and connected with a gauge operator to describe the coupling (see fig. 6). The gauge symmetries restrict the coupling of the mediator to the SM [3].

The four most common portals are shown in fig. 6. In this thesis, I will focus on the *Vector Portal* with its mediators *Dark Photons*. Its gauge operator is given with

$$-\frac{\epsilon}{2\cos\theta_W}B_{\mu\nu}F'^{\mu\nu} \quad (1)$$

where ϵ is the mixing parameter (or coupling constant) and θ_W is the weak mixing angle. $F'^{\mu\nu} = \partial_\mu A'_\nu - \partial_\nu A'_\mu$ is the Dark Photon field strength tensor, and $B_{\mu\nu} = \partial_\mu B_\nu - \partial_\nu B_\mu$ the hypercharge field strength tensor. The Dark Photon is the vector field A'_μ and will be further discussed in chapter 4.4 [3].

Portal	Particles	Operator(s)
“Vector”	Dark photons	$-\frac{\epsilon}{2\cos\theta_W}B_{\mu\nu}F'^{\mu\nu}$
“Axion”	Pseudoscalars	$\frac{a}{f_a}F_{\mu\nu}\tilde{F}^{\mu\nu}, \frac{a}{f_a}G_{i\mu\nu}\tilde{G}_i^{\mu\nu}, \frac{\partial_\mu a}{f_a}\bar{\psi}\gamma^\mu\gamma^5\psi$
“Higgs”	Dark scalars	$(\mu S + \lambda S^2)H^\dagger H$
“Neutrino”	Sterile neutrinos	$y_N LHN$

Figure 6: Different options for portals. Their mediator particles are written in the middle and their gauge operators on the right. Table is taken from [3]

A focus should be set on the coupling constant ϵ . It is called coupling constant or mixing parameter and gives the coupling strength of the mediator to SM matter. Finding a theoretical upper limit for ϵ will be the goal of this thesis.

4.4 Dark Photons

Dark Photons, U-Bosons, A' gauge bosons - no consistent term exists yet to describe one and the same thing. Regarding the notation, the expression U-Boson with index U will be used for calculations and the name Dark Photon occasionally in written text. In papers, equations are often labeled with A' , though.

Nonetheless, a better understanding of what a Dark Photon is will be necessary. Dark Photons are supposed to mediate the interaction between WIMPs and SM particles. Therefore, they need to couple to SM particles as described in the last chapter. Using the given gauge operator, Dark Photons can then be described with the following Lagrangian:

$$L_{A'} = -\frac{1}{4}F'^{\mu\nu}F'_{\mu\nu} + \frac{1}{2}\frac{\epsilon}{\cos\theta_W}B^{\mu\nu}F'_{\mu\nu} - m_{A'}^2 A'^\mu A'_\mu \quad (2)$$

The notation is the same as above, with the Dark Photon mass $m_{A'}$ [3]. Again, A'_μ is the Dark Photon. This *minimal kinetically mixed Dark Photon* already describes one of the simplest possible Dark Sectors for vector portals itself [3]. It can also represent a part of a larger Sector and easily be extended to one. Note that the mass of a Dark Photon is non-zero, albeit presently unknown.

The coupling to the SM allows Dark Photons to decay not only into DM particles but also into SM particles. To search for a Dark Photon, decays that take place via (ordinary) gauge photons are promising research approaches to find additional events that occur from the decay of Dark Photons into the same, measurable decay products. The following chapters will explain the search for Dark Photons in dilepton spectra and focus on searching for a Dark Photon. The predictions done in theory will then be used to find an upper constraint on the coupling constant ϵ .

5 Theoretical Approach

The goal of this thesis is to extract a theoretical upper limit for the coupling constant ϵ from possible U-Boson contributions in dilepton spectra. The results will be compared to the experimental results from the HADES experiment (details can be found in chapter 6). To calculate the dilepton spectra, the PHSD approach has been used, at first only calculating the contributions from SM sources. For further calculations, it was extended for U-Boson contributions. This chapter presents the obtained SM dilepton channels. In the following chapters, the experimental results and theoretical approaches will be explained, followed by the extension of PHSD with U-Bosons.

5.1 PHSD

PHSD (Parton Hadron String Dynamics) is an off-shell transport approach to describe the full evolution of a heavy-ion collision [15, 16]. It is based on the HSD (Hadron String Dynamics) model developed by the Universities of Frankfurt and Gießen. In the hadronic sector, PHSD is equivalent to HSD [17, 18].

The initial A+A collisions are implemented as in HSD: the string formation occurs in primary nucleus-nucleus collisions, followed by string decays into pre-hadrons (baryons B and mesons m). Here, strings are color-neutral excited objects formed by two partons. Their decay, called string-breaking, proceeds by the separation of the partons [19]. Afterwards, the formation of the quark-gluon plasma (QGP) stage is described, where the pre-hadrons dissolve:

$$B \rightarrow qqq \tag{3}$$

$$m \rightarrow q\bar{q} \tag{4}$$

to massive colored quarks q and antiquarks \bar{q} . The phase transition from pre-hadrons to QGP needs a consistent non-equilibrium (transport) model that explicitly describes parton-parton interactions and the phase transition from hadronic to partonic degrees of freedom, meaning that it follows lattice QCD for the partonic phase [20].

The formation of the QGP stage is based on DQPM (Dynamical Quasi-Particle Model) for partons. It is used to reproduce the effects of lattice QCD and results in a thermodynamical equilibrium. DQPM describes the properties of the interactions of quasi-particles (massive quarks and gluons) which are defined by DQPM with off-shell spectral functions such as widths and masses [20].

The transition from the QGP to the hadronic phase is then described by covariant transition rates for fusions of quark-antiquark pairs to mesonic resonances or three (anti-)quarks to baryonic states. The transport description of gluons and quarks is also based on DQPM. The hadronic phase is again equivalent to the off-shell HSD approach [17].

PHSD simulates the collision of two nuclei with specified energy and impact parameter. The impact parameter b determines whether a collision between two testparticles can take place or not. Its influence is studied in chapter 5.2.2. The total cross-section σ_{tot} defines the area of interaction. A collision then takes place when the impact parameter is lower than the acceptance given by the cross-section [21]:

$$b \leq \sqrt{\frac{\sigma}{\pi}} \tag{5}$$

So graphically spoken, the impact parameter gives information on how central a collision is (and thereby indirectly, how many particles are involved - see multiplicity plots in 5.2.2).

5.2 Studies of Au+Au collisions

Prior to the main task of calculating dilepton channels with PHSD, the rapidity distribution and p_T spectra of Au+Au at 1.23 GeV/A collisions were obtained.

5.2.1 Rapidity and Transverse Momenta

In heavy-ion collisions nuclear matter is present in a dense and hot state. As described above, this QCD matter is thought to be a QGP of strongly interacting quarks and gluons. The goal of heavy-ion collisions is then to describe the behavior of quarks and gluons under these extreme conditions. The *multiplicity* of charged particles in heavy-ion collisions is a way to describe the properties of this matter created in the collisions. To understand the contributions to particle production from both hard scattering and soft processes, the *rapidity distribution* and its dependence on energy and impact parameter are a suitable measurement.

The rapidity can be derived from the *pseudorapidity* η [22]. The pseudorapidity describes the angle between a particle and the beam axis:

$$\eta = -\ln \left(\tan \left(\frac{\theta}{2} \right) \right) \quad (6)$$

where θ is the angle between the three-momentum \mathbf{p} of the particle and the positive beam direction. According to this, the pseudo-rapidity can be re-written in terms of the three-momentum and longitudinal momentum:

$$\eta = \frac{1}{2} \ln \left(\frac{|\mathbf{p}| + p_L}{|\mathbf{p}| - p_L} \right) \quad (7)$$

Here, p_L is the longitudinal momentum.

For particle velocities close to the speed of light, the mass is neglected and the three-momentum replaced with the energy E . In this limit η is equivalent to the rapidity y .

$$y = \frac{1}{2} \ln \left(\frac{E + p_L}{E - p_L} \right) \quad (8)$$

The other important observable is the transverse momentum p_T .

$$p_T = \mathbf{p} \sin\theta \quad (9)$$

where θ is the particle emission angle [22].

The rapidity distribution and transverse momentum distribution for Au-Au collisions was calculated using PHSD.

The rapidity distribution of a Au+Au collision for protons and π^\pm , as well as its p_T spectra for $b = 2.25$ fm calculated with PHSD are presented in fig. 7.

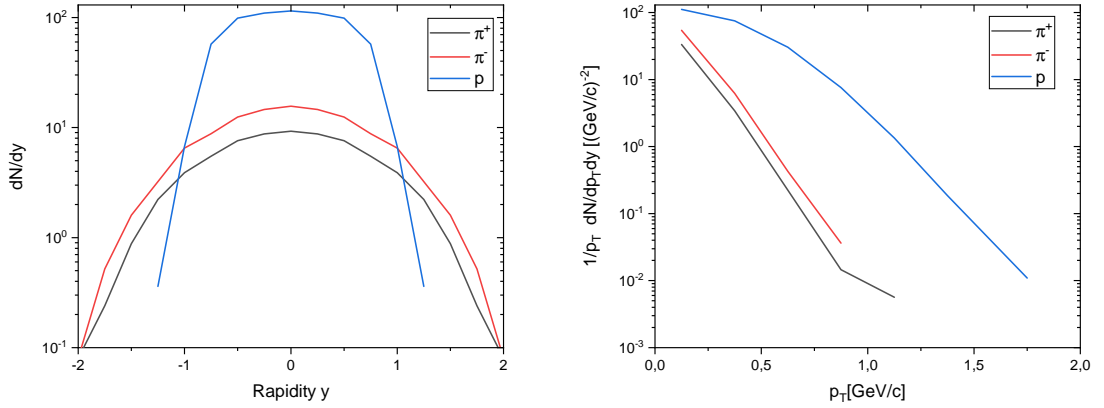


Figure 7: Left: Rapidity distributions for protons (p) and π^\pm for 1.23 A GeV Au+Au collisions at $b = 2.25$ fm. Right: Transverse momentum distributions for protons and π^\pm for 1.23 A GeV Au+Au collisions at $b = 2.25$ fm.

On the left the number of produced particles N is plotted against the rapidity y . For a central collision, the rapidity distribution in fig. 7 can be described with a gaussian curve. When looking at the centrality dependence later on, the gaussian shape will be distorted.

5.2.2 Centrality and Impact Parameter

As a next step, the centrality dependence of hadron productions was studied. For that, collisions for differing impact parameters b in a range from $b_{min} = 0.25$ fm to $b_{max} = 14.5$ fm were simulated. As explained in 5.1, the impact parameter gives the distance between the centre of the nuclei.

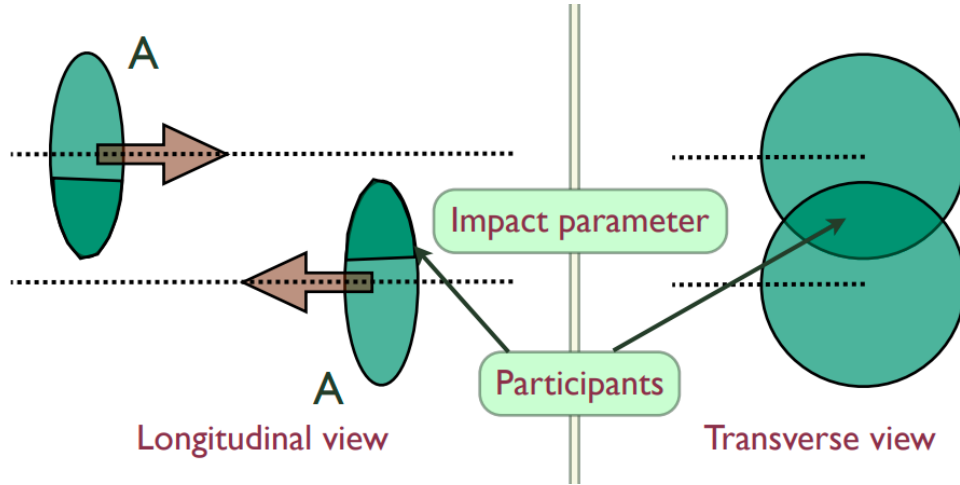


Figure 8: Graphical description of the impact parameter. The larger b , the less central the collision and the less participants contribute to the collision. Figure is taken from [23].

According to this, less particles should participate with increasing impact parameter.

The influence of the centrality can also be seen in the particle multiplicity. It gives information on the centrality and the energy density of a collision and scales with the number of participants N_{part} . The multiplicity distribution shows the number of produced particles as a function of participants. The influence of the centrality is quite clear: the more central a collision, the more participants contribute. In experiment, the centrality of a collision cannot be determined directly. The multiplicity therefore is an important observable to make statements on the centrality.

The number of participants N_{parts} in dependence on the centrality is shown on the left side of fig. 9. The impact parameter was increased with equidistant steps (0.25 fm). The number of participants vs the total particle number is shown for this case in the right plot of fig. 9 that shows the multiplicity.

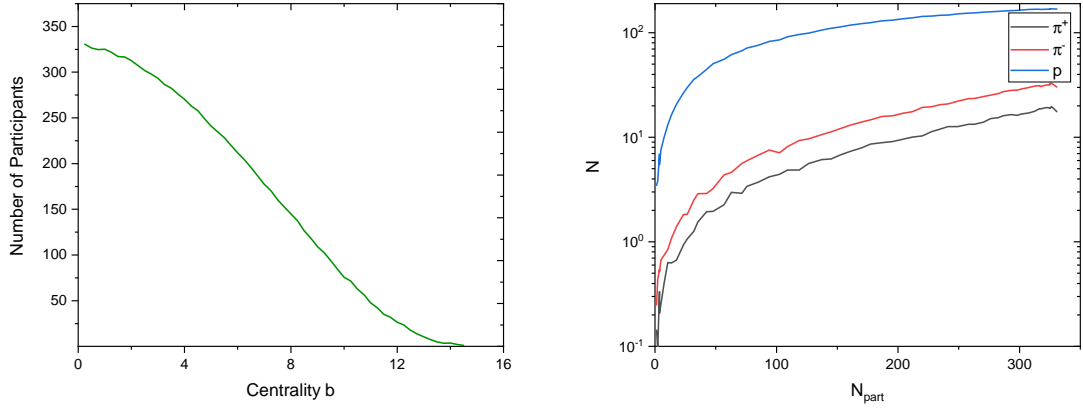


Figure 9: Left: Number of participants in dependence on centrality b in Au+Au collisions at 1.23 A GeV. Right: Multiplicities for protons and π^{\pm} in Au+Au collisions at 1.23 A GeV vs N_{part} .

The effect of an increasing impact parameter becomes very clear from the left plot of fig. 9: going to a maximum impact parameter of 14.5 fm, the number of participating particles reaches its maximum at the most central collision and decreases with larger b . The number of produced particles depends on the number of participants. The more particles participate in the collision, the more charged particles are produced as follows from fig. 9. There, the number of hadrons increases with N_{part} from peripheral to central collisions.

The effect of the centrality selection by changing the impact parameter on the rapidity distribution and p_T spectra can be seen in fig. 10. The collision at $b = 10$ fm is much more peripheral than at $b = 2.25$ fm shown in fig. 7. According to this, less participants should be involved.

The p_T spectra keep their shape but are smaller in general.

We show the resulting p_T and rapidity spectra for $b = 10.0$ fm in fig. 10.

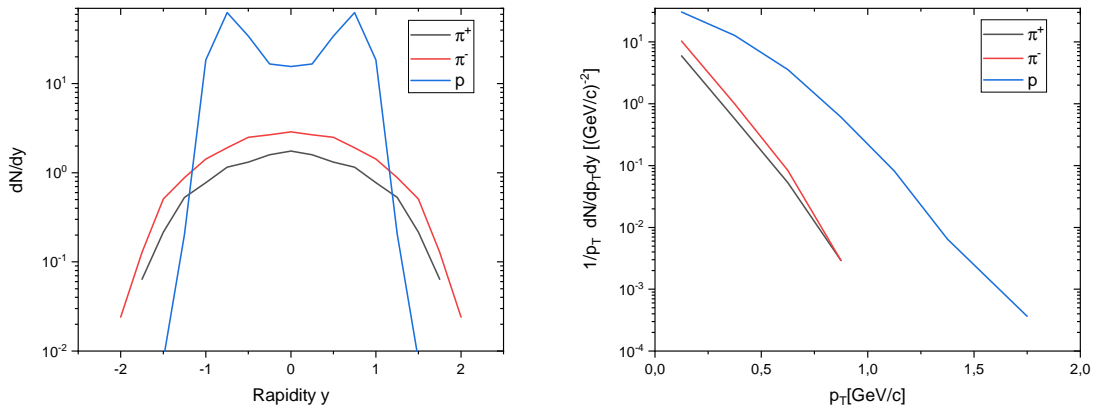


Figure 10: Rapidity distributions for protons (p) and π^\pm for 1.25 A GeV Au+Au collisions at $b = 10.0$ fm. Right: Transverse momentum distributions for protons and π^\pm for 1.25 A GeV Au+Au collisions at $b = 10.0$ fm.

The height of the rapidity distributions depends on the centrality. The total number of produced particles is proportional to the number of participants, that is centrality dependent, as shown in fig. 9. Therefore, also the rapidity distributions are smaller for less central collisions. The p_T spectra become smaller for the same reasons.

The Au+Au collisions at 1.23 A GeV for differing impact parameters b were calculated, where b was increased with constant steps of 0.25 fm in a range $[b_{min}, b_{max}] = [0.25 \text{ fm}, 14.5 \text{ fm}]$. The results are presented in fig. 11.

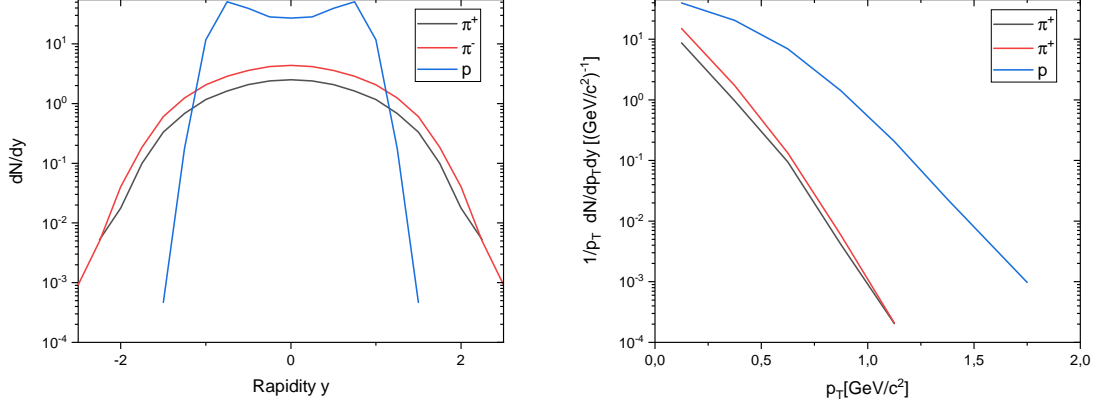


Figure 11: Left: Rapidity distribution for protons p and π^\pm for 1.23 A GeV Au+Au collisions for $b = [0.25, 14.5]$ fm. Right: Transverse momentum distributions for protons and π^\pm for 1.23 A GeV Au+Au collisions for $b = [0.25, 14.5]$ fm. b is increased with a constant step of 0.25 fm.

The rapidity distributions and p_T spectra above are averaged over a centrality range $b = [0.25, 14.5]$ fm. Therefore, they are smaller than merely very central collisions at $b = 2.25$ fm (fig. 7), but noticeably larger than a single semi-peripheral collision at $b = 10$ fm (fig. 10).

With the knowledge of these basics, the production of dileptons, that will be important to find Dark Photons, can be studied.

5.3 Dilepton Sources

Dileptons are a unique probe for nuclear matter in heavy-ion collisions. They are emitted from different stages of a heavy-ion reaction and not affected by final-state interactions. Thereby, they give clear information about the production channels. The dilepton spectra can be calculated theoretically based on a microscopic transport approach.

5.3.1 General

In this thesis, I will focus on dilepton sources from meson and baryon decays, meaning direct decays and especially Dalitz decays. The decays of mesons into dileptons (in this case, dielectrons e^+e^-) are direct decays or Dalitz decays. In both cases a virtual photon γ^* decays into a lepton pair l^+l^- (here, e^+e^-):

$$\gamma^* \rightarrow l^+l^- \quad (10)$$

A virtual photon has a defined mass m_{γ^*} that is non-zero:

$$m_{\gamma^*}^2 = q^2 - q_0^2 = (p_{e^+} + p_{e^-})^2 > 0 \quad (11)$$

Dileptons provide a lot of information to study meson properties such as mass and electromagnetic decay widths.

The differential branching ratios from hadron decays are given by

$$\frac{dB(\mu, M)}{dM} = \frac{1}{\Gamma_{tot}(\mu)} \frac{d\Gamma(\mu, M)}{dM} \quad (12)$$

where μ is the hadron mass and M the dilepton mass. The branching ratio provides the fraction of particles which decay by a specific decay mode against the total number of decaying particles.

5.3.2 Direct Decay

The decay of a vector meson (ρ, ω, ϕ) into a dilepton pair occurs via a virtual photon which is indicated by the diagram in fig. 12.

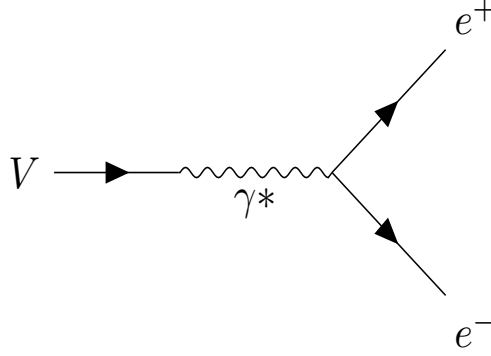


Figure 12: Direct decay of a vector meson into a dielectron pair via a virtual photon γ^* .

In general, the decays of vector mesons via a direct decay are

$$\rho \rightarrow e^+e^- \quad (13)$$

$$\omega \rightarrow e^+e^- \quad (14)$$

$$\phi \rightarrow e^+e^- \quad (15)$$

Since this thesis focuses on the Dalitz decays of π^0 , η , and Δ via U-Bosons, the direct decay of vector mesons is only important for the remaining background channels presented in the dilepton spectra. The production of Dark Photons will follow from Dalitz decays which are described in detail in the following subchapter.

5.3.3 Dalitz Decay

Fig. 13 shows the diagram for the Dalitz Decay of a scalar meson or pseudoscalar meson to a dilepton pair and an additional photon.

$$B \rightarrow \gamma + l^+l^- \quad (16)$$

Initially, the meson decays into a photon γ and a virtual photon γ^* . The virtual photon then decays further in an electron-photon interaction into the dilepton pair (dielectron).

The simplest examples are the decays of pions and η mesons into a photon and an electron-positron pair:

$$\pi^0 \rightarrow \gamma\gamma^* \rightarrow \gamma + e^+e^- \quad (17)$$

$$\eta \rightarrow \gamma\gamma^* \rightarrow \gamma + e^+e^- \quad (18)$$

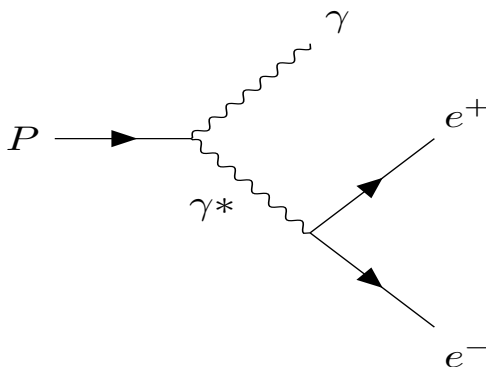


Figure 13: Dalitz decay of a pseudoscalar meson (π^0 or η) via a virtual photon γ^* into a dielectron pair while emitting another photon γ .

The Dalitz decay of a baryonic Δ resonance

$$\Delta \rightarrow N\gamma^* \rightarrow N + e^+e^- \quad (19)$$

is shown in fig. 14. Dalitz decays become important again when talking about decays via Dark Photons in 7.1. In 5.5, the calculated dilepton spectra from SM channels using PHSD are presented.

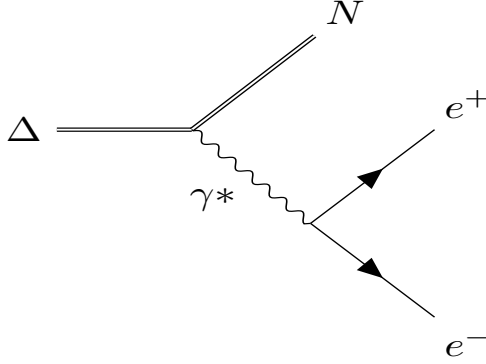


Figure 14: Dalitz decay of a Δ resonance via a virtual photon γ^* into a dielectron pair.

5.4 Dilepton Spectra

Measuring a single Dark Photon contribution is not possible. Instead, all SM channels must be included as a background. The Dark Photon contribution (if it exists) might then be visible as an excess above this background.

The background created by SM particles has been calculated and compared with experimental data from the HADES experiment. Note that for p+p and p+Nb reactions the differential cross-sections $d\sigma/dM$ are plotted in dependence on the invariant dilepton mass M at 3.5 GeV [24, 25, 26], while for Ar+KCl the invariant mass spectra dN/dM normalized for the number of pions N_{π^0} at 1.76 A GeV is plotted [27]. The results of PHSD calculations for dilepton spectra including HADES acceptance are shown in figs. 15 - 17. The result of the background calculations are the dilepton spectra for p+p, p+Nb, and Ar+KCl collisions including all possible SM channels. The spectra are dominated by π^0 , η , and Δ contributions at lower masses. Other contributions show up mainly at higher masses. Note that the Δ contribution accesses higher masses than π^0 and η .

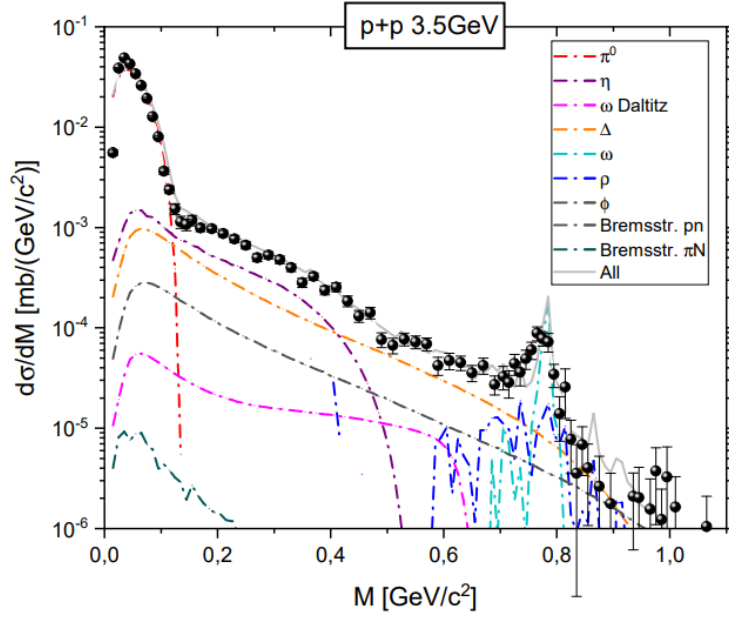


Figure 15: Differential cross-section $d\sigma/dM$ for e^+e^- production in p+p reactions at 3.5 GeV beam energy. The theoretical calculation from PHSD is compared to HADES data [26]. The different color lines display individual channels in the transport calculation (see legend).

Fig. 15 shows the differential cross-section $d\sigma/dM$ from PHSD calculations for e^+e^- production at a beam energy of 3.5 GeV. The black dots represent the HADES data [26] to which the theoretical calculations are compared. The grey line, which is the sum of all contributions, agrees well with the HADES experimental data.

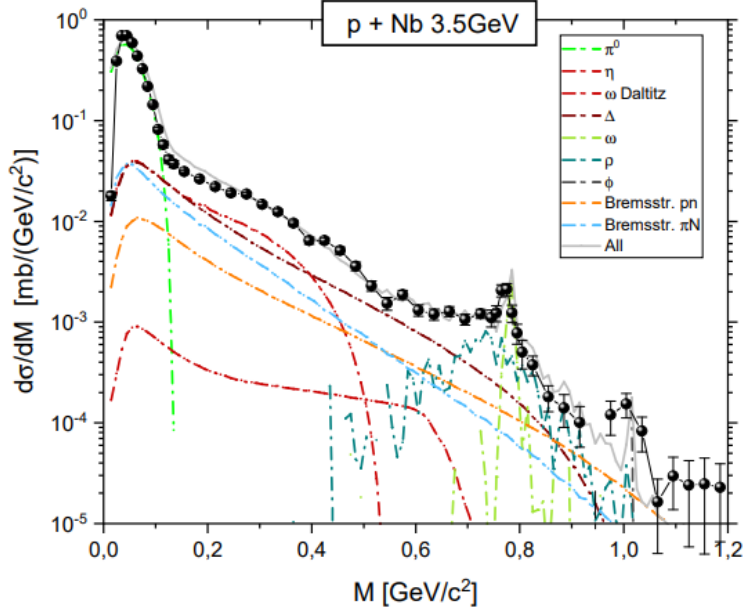


Figure 16: Differential cross-section $d\sigma/dM$ for e^+e^- production in p+Nb reactions at 3.5 GeV beam energy. The theoretical calculation from PHSD is compared to HADES data [24, 25]. The different color lines display individual channels in the transport calculation (see legend).

Fig. 16 shows the differential cross-section $d\sigma/dM$ from PHSD calculations for e^+e^- production at a beam energy of 3.5 GeV. Again, the HADES data [24] are plotted as black dots. The grey line that presents the sum of all theoretically calculated contributions lies well on the experimental data.

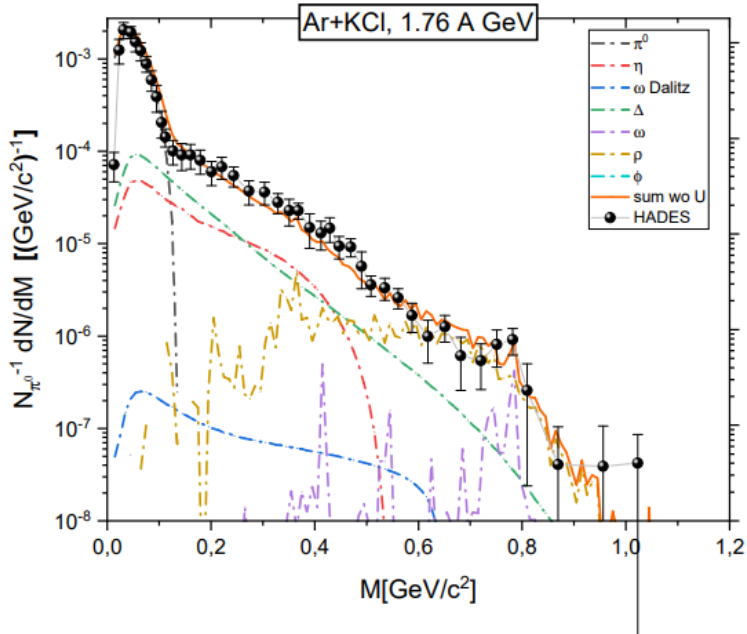


Figure 17: Mass differential dilepton spectra dN/dM normalized to π^0 multiplicity for Ar+KCl reactions at 1.76 A GeV and $b = 0.5 - 6.0$ fm centrality. The theoretical calculation from PHSD is compared to HADES data [27]. The different color lines display individual channels in the transport calculation (see legend).

Fig. 17 shows the invariant mass spectra dN/dM for Ar+KCl reactions, normalized to the π^0 multiplicity. Note that the impact parameter b lies within a range of 0.5-6.0 fm. As follows from figs. 15 - 17, the present calculations agree very well with HADES data and previous PHSD calculations as from [28]. These plots provide the theoretically obtained background for later dilepton spectra that include U-Boson contributions.

6 Experimental Dilepton Spectra

6.1 The HADES experiment

HADES (**H**igh **A**cceptance **D**i**E**lectron **S**pectrometer) at GSI Helmholtzzentrum für Schwerionen in Darmstadt measures dilepton spectra produced in collisions at beam energies between 1 GeV and 3.5 GeV. It uses beams produced by the SIS18 ring accelerator.

The measured dilepton spectra from HADES are used to search for evidence for Dark Photons. HADES searches for the decays of Dark Photons to e^+e^- in inclusive dilepton spectra. Using spectra from different reactions (see chapter 6.2), an experimental upper limit for the kinetic mixing parameter ϵ^2 has been obtained with an acceptance of 90%. Prior to understanding the experiments on the search for Dark Photon decays, the measurements of SM dilepton spectra and their results are discussed. More detailed information on the spectra and expectations will be given to make use of the results and compare them to the later presented theoretical calculations.

6.2 Dilepton Sepctra by HADES

HADES measures inclusive spectra coming from all dilepton channels. The experiments were done for a proton beam at 3.5 GeV with a liquid hydrogen target (p+p) and a solid niobium target (p+Nb), and an Argon beam at 1.76 GeV/u with a KCl target. The spectra for all reactions (that are not corrected for efficiency and acceptance) are presented in fig. 18.

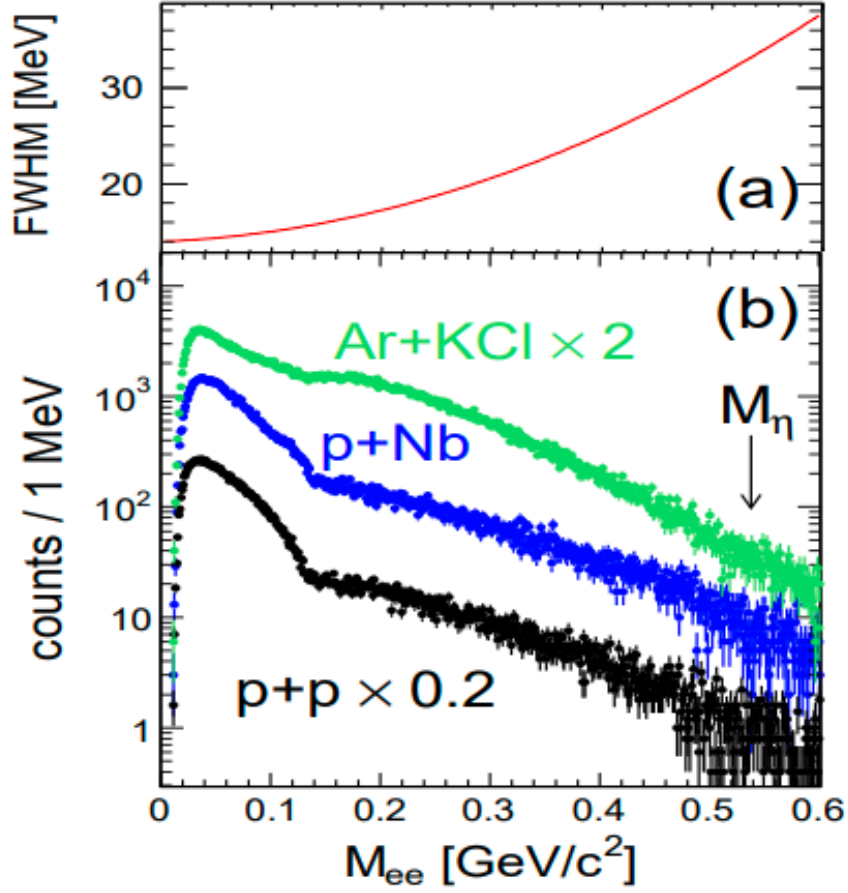


Figure 18: (a) Dielectron mass resolution (FWHM) as a function of the e^+e^- invariant mass obtained from a Monte-Carlo simulation. (b) Inclusive dilepton spectra from HADES experiment for Ar+KCl at 1.76 A GeV, p+p, and p+Nb at 3.5 GeV with statistical error bars. The plot is taken from [29].

M_η indicates the position where a peak caused by a direct η decay would occur ($M_\eta = 0.548$ GeV/c^2). The peak is not visible, but an upper limit can be extracted at this position.

6.3 Measuring Techniques for invisible particles

In this subchapter, the experimental measuring techniques to find DM contributions caused by Dark Photons are explained, and the HADES expectations are presented. Following these, the theoretical calculations and final results of this thesis are shown.

When using heavy-ion collisions, a beam with fixed energy and momentum is sent towards a target. After it hits the target, the decay products move away in different directions and carry a part of the initial momentum with them.

The important fact is now that the initial momentum of the beam is carried along only one axis. After the collision, it splits up and is carried away by the decay products in any direction. Nonetheless, the sum of all momenta should still be the initial momentum. But if an invisible particle is produced in some way, it will carry away the momentum undetected. So after summing up all remaining momenta, the outcome will be smaller than expected - and one knows he found an invisible particle.

Another option is that unknown particles are produced and decay into known particles again. For that case, the number of events is counted, and if a decay takes place that is not yet known, one will see it as an additional signal in the counting. In the case of Dark Photons, this approach is applied by HADES, and a whole dilepton spectrum are measured. So if a Dark Photon would decay to e^+e^- , HADES would observe a peak structure in the measured spectrum.

6.3.1 Excess in Dilepton Spectra

In the specific case of the HADES spectra, searching for a peak means a search for a narrow resonance on top of the spectra presented in fig. 18. The sharp peak should occur on top of a spectrum at the point of the U-Boson mass. The mass of a U-Boson is unknown, and therefore, it is impossible to make a theoretical prediction where the peak would be visible. Instead, the whole mass range of the dilepton spectra is taken into account, leading to an expected contribution at any point and, thereby, to a smooth curve instead of a sharp peak. As expected, the curve lies above the measured spectra, but cannot overshoot the measured spectra by more than a given confidence level.

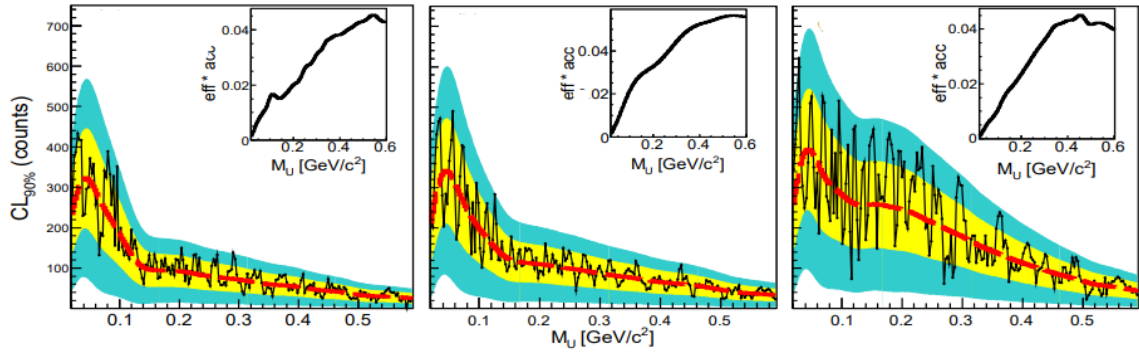


Figure 19: Extracted 90% confidence level (Confidence Level) upper limits for a narrow $U \rightarrow e^+e^-$ signal found by HADES for p+p (left), p+Nb (middle) and Ar+KCl (right). Pink line: computed experimental sensitivity. The error bands are printed in yellow (1σ) and blue (2σ). The expected excess in the number of counts is plotted for a 90% CL against the U-Boson mass M_U . The plot is taken from [29].

Fig. 19 shows the HADES expectations for U-Boson signals obtained by simulations employing a narrow peak of fixed position M_{ee} on top of a 5th order polynomial [29]. The expected signals from HADES are printed as a black solid line that lies mainly within a 1σ confidence level. However, especially for ArKCl, the expectations go into a 2σ confidence level of over 90%.

7 Finding a Dark Photon

Particle Colliders such as HADES provide exciting approaches to search for a Dark Photon. But - how does one search for a particle that is invisible by definition? In the following chapter, I will give some insights to this question.

7.1 Interaction

The idea is to search for the dilepton decay of a U-Boson ($U \rightarrow e^+e^-$). According to the assumed mass M_U of the U-Boson the decay will be visible at this point of the mass distribution of e^+e^- pairs.

A U-Boson can be produced in the decay of pseudoscalar mesons

$$\pi^0 \rightarrow U\gamma \rightarrow \gamma + e^+e^- \quad (20)$$

$$\eta \rightarrow U\gamma \rightarrow \gamma + e^+e^- \quad (21)$$

$$(22)$$

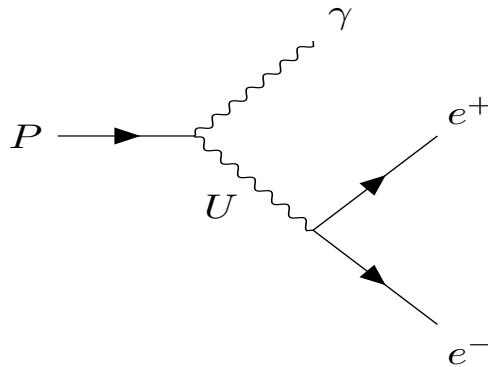


Figure 20: Dalitz decay of a vector meson (π^0 or η) via a U-Boson U into a dielectron pair while emitting another photon γ .

The decay of Δ resonances proceeds as follows:

$$\Delta \rightarrow NU \rightarrow N + e^+e^- \quad (23)$$

The corresponding diagram for the decays of π^0 and η are shown in fig. 20, the diagram for the decay of a Δ resonance in fig. 21. The mass of a U-Boson is unknown, as well as its coupling to SM matter.

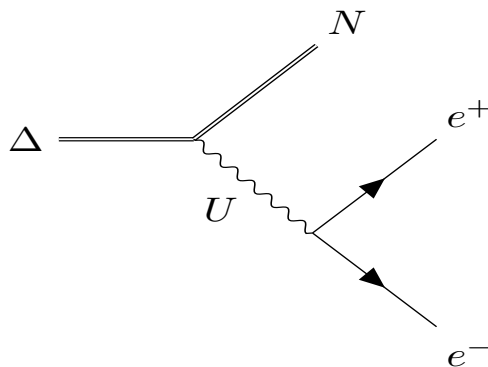


Figure 21: Dalitz decay of a Δ resonance via a U-Boson U into a dielectron pair.

7.1.1 The role of the Mixing Parameter

The mixing parameter ϵ^2 restricts possible U-Boson contributions to the total SM decay contributions with a given confidence level. For HADES, this level is 90%, as shown in fig. 19. Using these simulations, the mixing parameter can be extracted from the data. Fig. 23 shows the resulting ϵ^2 values in dependence on the mass of a U-Boson obtained by HADES.

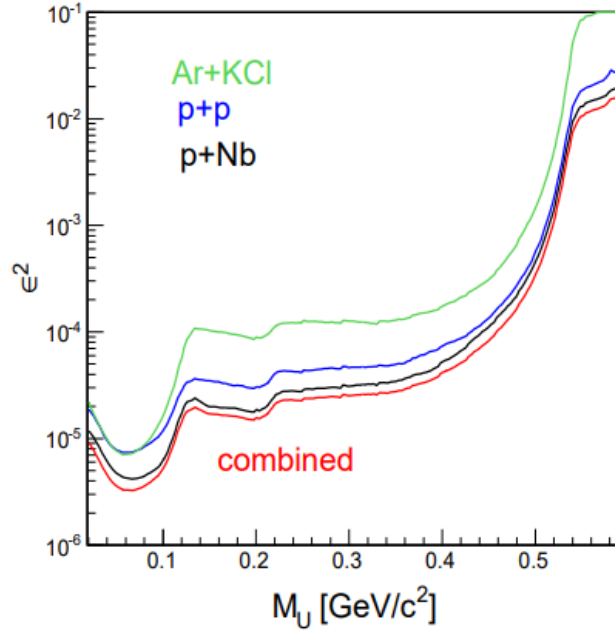


Figure 22: HADES ϵ^2 from Ar+KCl, p+p, and p+Nb spectra in dependence on the U-Boson mass M_U . Figure is taken from [29].

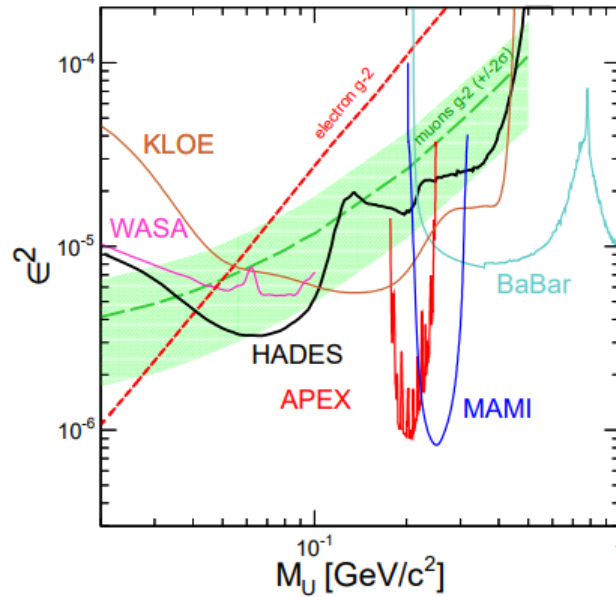


Figure 23: Comparison of combined ϵ^2 results with other experiments. Figure is taken from [29].

Fig. 23 presents results for an upper limit for ϵ^2 from different experiments at masses M_U between 0 and $1 \text{ GeV}/c^2$ and in an ϵ^2 range between 10^{-6} and 10^{-4} . The HADES prediction for ϵ^2 lies within that range. At low masses, the HADES result improves on the WASA result, at higher masses, it is very similar, albeit slightly lower than the KLOE results.

7.2 Theoretical Calculations

This chapter aims to present the theoretical implementation of U-Boson production and decay to dileptons in the PHSD approach. From this, the contributions from π^0 , η and Δ decays via U-Bosons can be calculated and summed to a total U-Boson contribution. Analogously to experiment, a confidence level will be given, and from this, the upper limit for the mixing parameter can be extracted, as will be explained in chapter 8.

7.2.1 Implementing U-Boson contributions in the PHSD

The decays of U-Bosons will add new contributions to the spectra and thereby change the total sum of all contributions. The goal will be to calculate such U-Boson contributions and add them to the background. The total sum shall not overshoot the sum of only the

SM contributions by more than 20%, such that theoretical results stay on the upper level of the experimental error bars for the dilepton spectra. This can be achieved varying ϵ^2 - meaning it has to be extracted from the calculated spectra.

So the first step is to calculate the U-Boson contributions. As shown in the last chapter, the dilepton spectra at $M < 0.56 \text{ GeV}/c^2$ are dominated by π^0 , η , and Δ channels. Therefore, I only calculated the new U-Boson contributions for these three channels.

At first, it is convenient to look at the branching ratio for the decay of U-Bosons to e^+e^- as in ref. [29]:

$$BR_{ee} = \frac{\Gamma_{U \rightarrow ee}}{\Gamma_{tot}} = \frac{1}{1 + \sqrt{1 - \frac{4m_\mu^2}{M_U^2}} \left(1 + \frac{2m_\mu^2}{M_U}\right) (1 + R(M_U))}. \quad (24)$$

Here, $\Gamma_{tot} = \Gamma_{hadr} + \Gamma_{ee} + \Gamma_{\mu\mu}$ with $\Gamma_{\mu\mu} = \Gamma_{ee}$ for $M_U \gg 2m_\mu$ due to lepton universality. M_U is the U-Boson mass, m_μ the lepton mass and $R(M_U) = \sigma_{e^+e^- \rightarrow hadrons} / \sigma_{e^+e^- \rightarrow \mu^+\mu^-}$ is chosen such that $R(M_U) \Gamma_{\mu\mu} = \Gamma_{hadr}$. The branching ratio will later be used to calculate the η and Δ dilepton decay widths, as described in 5.4.1.

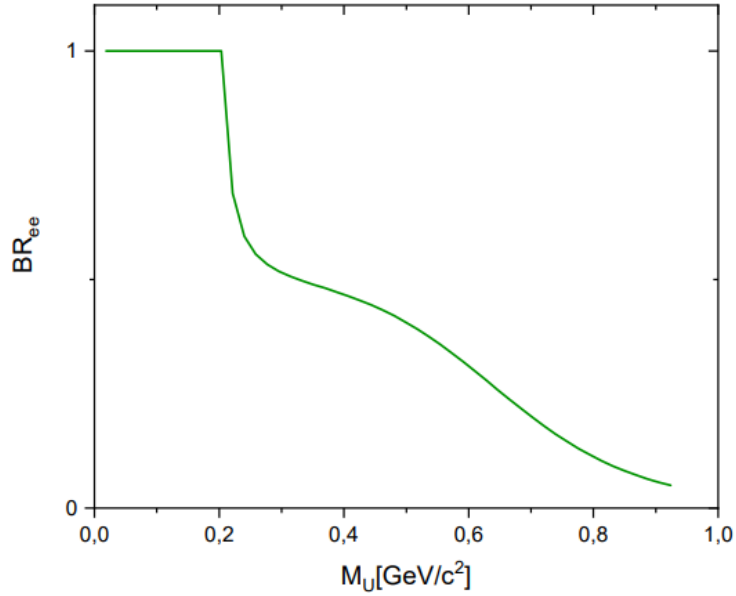


Figure 24: Branching ratio vs M_U [29].

Fig. 24 shows the Branching ratio for the decay of a U-Boson into a dielectron pair as a function of M_U . As one can see, the fraction is 1 at masses below $0.2 \text{ GeV}/c^2$. The mass of π^0 does not access masses higher than that, while both η and Δ do. Therefore, their electromagnetic decay widths need to be corrected using the branching fraction, while π^0 will not be influenced.

To calculate the U-Boson contributions, the decays of π^0 , η , and Δ to U-Bosons must be implemented in the PHSD code and calculated numerically. Following ref. [29], these are realised for η and π^0 by their partial decay widths to U-Bosons

$$\frac{\Gamma_{i \rightarrow \gamma U}}{\Gamma_{i \rightarrow \gamma \gamma}} = 2\epsilon^2 |F_i(q^2 = M_U^2)| \frac{\lambda^{3/2}(m_i^2, m_\gamma^2, M_U^2)}{\lambda^{3/2}(m_i^2, m_\gamma^2, m_\gamma^2)} \quad (25)$$

where ϵ^2 is the mixing parameter and λ is the triangle function for relativistic kinematics:

$$\frac{\lambda^{3/2}(m_i^2, 0, M_U^2)}{\lambda^{3/2}(m_i^2, 0, 0)} = \left(1 - \frac{M_U^2}{m_i^2}\right)^3 \quad (26)$$

and F_i are the electromagnetic transition formfactors for π^0 and η :

$$|F_{\pi^0}(q^2)| = 1 + 0.032 \frac{q^2}{m_{\pi^0}^2} \quad (27)$$

$$|F_\eta(q^2)| = \left(1 - \frac{q^2}{\Lambda^2}\right)^{-1} \quad (28)$$

with $\Lambda = 0.72 \text{ GeV}$.

Since Δ is a broad state, it has to be treated differently: the masses have to be integrated over the Δ spectral function $A(m_\Delta)$.

$$\frac{\Gamma_{\Delta \rightarrow NU}}{\Gamma_{\Delta \rightarrow N\gamma}} = \epsilon^2 \int A(m_\Delta) |F_\Delta(M_U^2)| \frac{\lambda^{3/2}(m_\Delta^2, m_N^2, M_U^2)}{\lambda^{3/2}(m_\Delta^2, m_N^2, 0)} dm_\Delta \quad (29)$$

where $A(m_\Delta)$ is the Δ mass distribution with the mass of Δ m_Δ , m_N the mass of the remaining nucleon. For Δ resonances, $|F_\Delta(q^2)| = 1$ is an appropriate choice that does not influence the results since an experimental formfactor is unknown [29].

$$\frac{\lambda^{3/2}(m_\Delta^2, m_N^2, M_U^2)}{\lambda^{3/2}(m_\Delta^2, m_N^2, 0)} = \left(1 - \frac{M_U^2}{m_\Delta^2}\right)^3 \quad (30)$$

The numerical calculation was done in Fortran. Since ϵ^2 is unknown, it was firstly set to 1 for the calculation of the decay widths. Its actual value will be obtained later from the spectra. A numerical calculation of the partial decay widths of π^0 , η and Δ resonance to a U-Boson are presented in fig. 25 and 26.

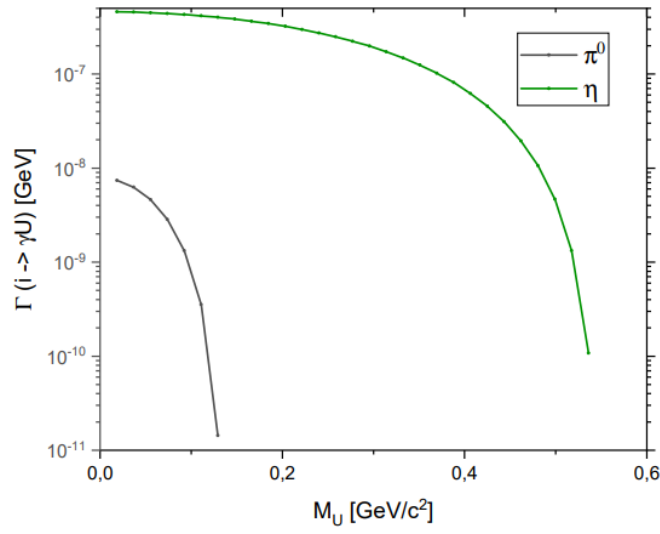


Figure 25: Decay widths Γ of π^0 and η to $U+\gamma$ for $\epsilon^2 = 1$.

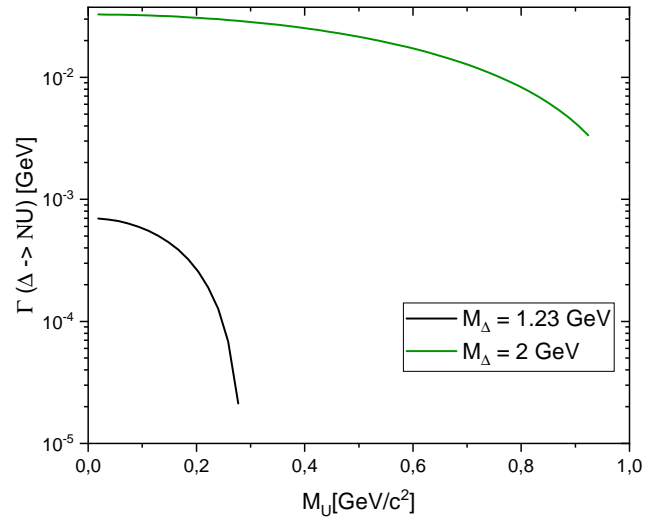


Figure 26: Decay widths of Δ resonances to N+U for $M_\Delta = 1.23$ GeV and $M_\Delta = 2$ GeV at $\epsilon^2 = 1$.

As expected, the decay widths of Δ resonances with large masses from U-Bosons are much larger than those with lower masses as well as π^0 and η .

Fig. 27 shows the decay widths of π^0 and η to a U-Boson multiplied with ϵ^2 from HADES that was presented in fig. 23.

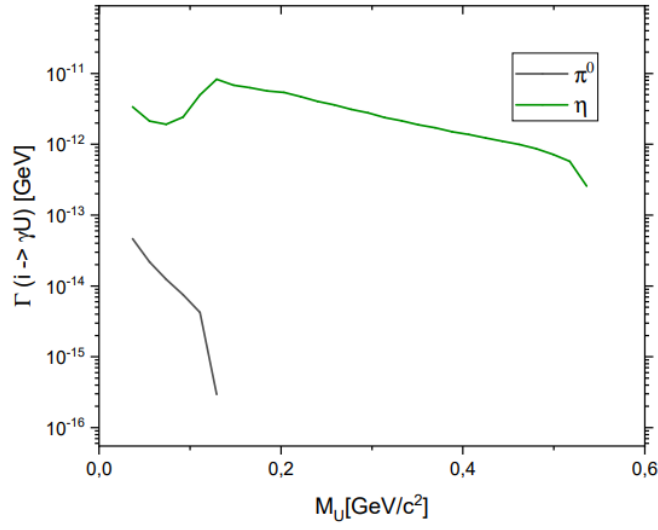


Figure 27: Decay widths of π^0 and η to $U+\gamma$.

Fig. 28 shows the decay widths of Δ resonances at $M_\Delta = 1.23$ GeV and $M_\Delta = 2$ GeV to a U-Boson multiplied with ϵ^2 from HADES.

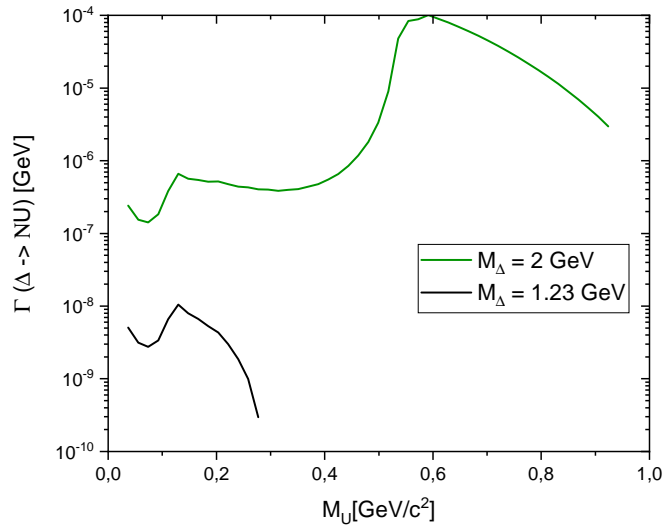


Figure 28: Decay widths of Δ resonances to $U+N$ at $M_\Delta = 1.23$ GeV and $M_\Delta = 2$ GeV.

Especially for η and Δ the influence of the coupling constant becomes obvious as it causes

larger changes in the decay widths.

8 The Goal: finding an upper limit for ϵ^2

As already explained, the total sum of SM channels and U-Boson contributions cannot overshoot the sum of SM channels by more than 20%. This is more understandable when formulated in an equation:

$$\frac{dN^{total}}{dM} = \frac{dN^{sumSM}}{dM} + \epsilon^2 \frac{dN^{sumU}}{dM} \quad (31)$$

The first term on the right side of the equation describes the total invariant mass from all SM channels, as presented in chapter 7.5. The last term adds then the channels caused by U-Boson decays - these need to be multiplied with the coupling constant ϵ^2 that restricts them such that they do not lay more than 20% above the sum of SM channels.

Using the decay widths which are presented in chapter 7.3, the U-Boson contributions for π^0 , η , and Δ can be calculated. The contributions were found for $\epsilon^2 = 1$ and, as expected, far too high above the total sum and HADES data. To correct the signal, it is multiplied with the coupling constant ϵ^2 that was calculated as follows:

$$\epsilon^2 = 0.2 \cdot \left(\frac{dN^{sumSM}}{dM} \right) / \left(\frac{dN^{sumU}}{dM} \right) \quad (32)$$

The pre-factor 0.2 arises from the chosen accuracy of 20%.

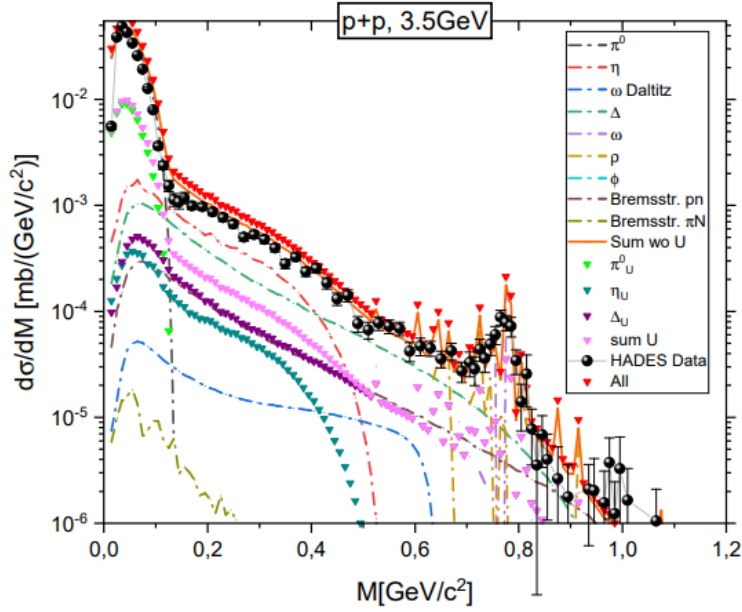


Figure 29: Differential cross-section $d\sigma/dM$ for e^+e^- production in p+p reactions at 3.5 GeV beam energy. The theoretical calculation from PHSD is compared to HADES data [26]. The different color lines display individual channels in the transport calculation (see legend). Included are the contributions from potential $U \rightarrow e^+e^-$ are shown as red triangles.

Fig. 29 presents the differential cross-section $d\sigma/dM$ from PHSD calculations for e^+e^- production including the implemented decays of π^0 , η , and Δ via U-Bosons. The contributions from the Dalitz decays of π^0 , η and Δ via U -bosons are indicated by colored triangles due to the fact that the exact mass of a U-Boson is unknown. One can see that the total sum of all ordinary channels and all U-Boson channels lies above the sum of all ordinary channels. The difference is never larger than 20%, as imposed. The corresponding mixing parameter ϵ subtracted from this calculation is presented in chapter 8.1.

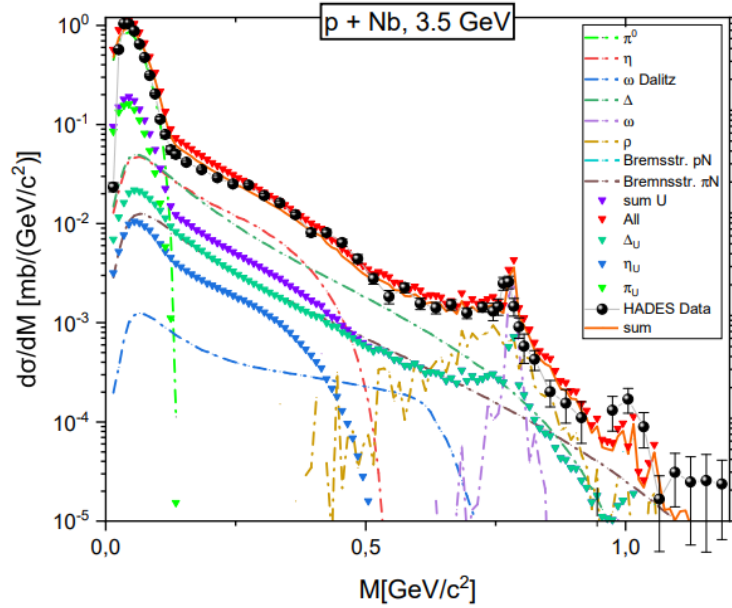


Figure 30: Differential cross-section $d\sigma/dM$ for e^+e^- production in p+Nb reactions at 3.5 GeV beam energy. The theoretical calculation from PHSD is compared to HADES data [24, 25]. The different color lines display individual channels in the transport calculation (see legend). Included are the contributions from potential $U \rightarrow e^+e^-$ are shown as red triangles.

Fig. 30 presents the differential cross-section $d\sigma/dM$ from PHSD calculations for e^+e^- production including the implemented decays of π^0 , η , and Δ via U-Bosons. As before, the contributions from the Dalitz decays of π^0 , η and Δ via U -bosons are indicated by colored triangles. The total sum of all ordinary channels and U-Boson channels does not exceed the total ordinary sum more than 20%. The subtracted ϵ^2 is shown in fig. 32.

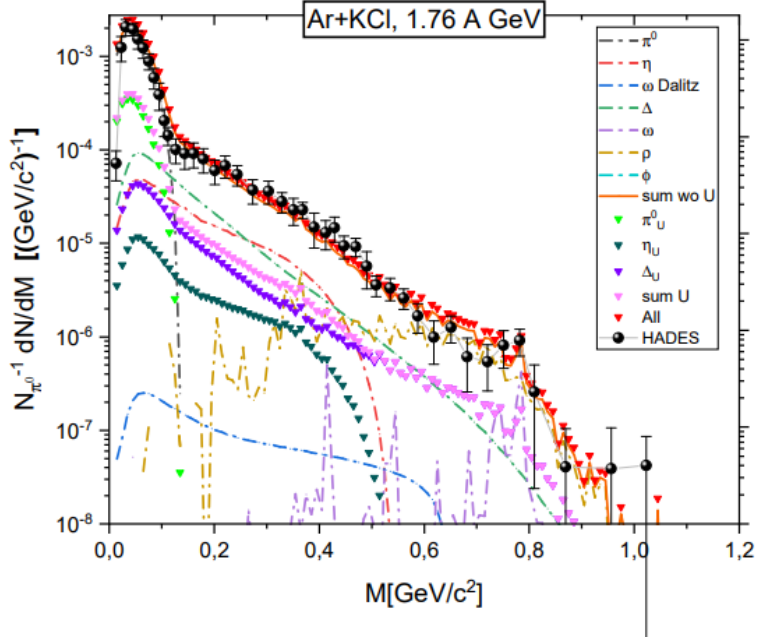


Figure 31: Mass differential dilepton spectra dN/dM normalized to π^0 multiplicity for Ar+KCl reactions at 1.76 A GeV and $b = 0.5 - 6.0$ fm centrality. The theoretical calculation from PHSD is compared to HADES data [27]. The different color lines display individual channels in the transport calculation (see legend). Included are the contributions from potential $U \rightarrow e^+e^-$ are shown as red triangles.

The results in fig. 31 show the calculated U-Boson contributions as discrete symbols to remind of the unknown U-Boson mass. Again, if a U-Boson contribution were detected in experiment, a sharp peak would be visible!

The total sum is represented as a red line of triangles. It lies not more than the given 20% above the total SM contribution and measured HADES data, as imposed. The single contributions from π^0 , η and Δ Dalitz decays to e^+e^- via U-Bosons are smaller than the according SM channels.

The mixing parameter ϵ^2 that was extracted from the theoretical calculations is presented in fig. 32.

8.1 Resulting ϵ^2

The final theoretical results for the mixing parameter ϵ^2 are shown in figure 32 and plotted in comparison with the result found by HADES (green line) [29].

The theoretical ϵ^2 at $M = 0.2 - 0.4 \text{ GeV}$ is close to the HADES expectation, albeit it is larger at lower M . This occurs from the fact that the HADES ϵ^2 was extracted from measurements that are not efficiency corrected. The theoretical results are smaller than the HADES results at higher masses. HADES does not access masses above $0.55 \text{ GeV}/c^2$. We note that theoretically found ϵ^2 at masses above that are not sufficiently accurate since the spectra are dominated by π^0 , η and Δ only at lower masses. At higher masses also ρ and ω contributions need to be taken into account, which was not part of this thesis.

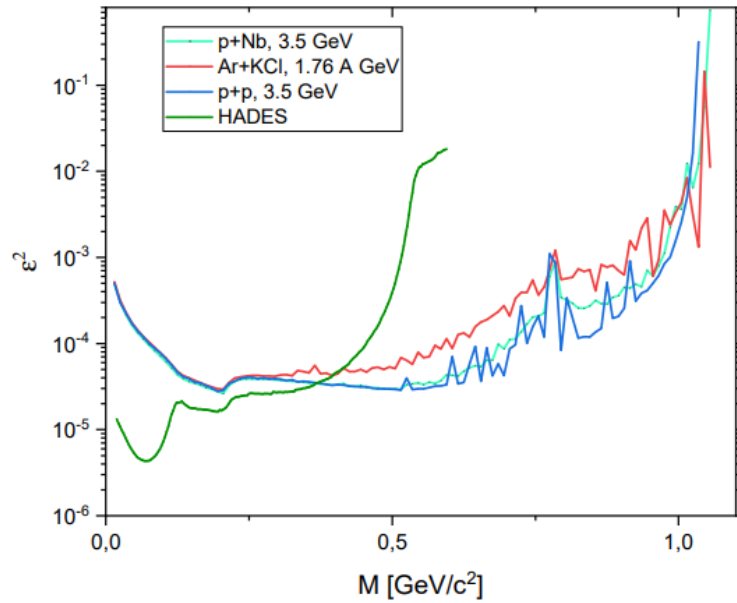


Figure 32: Theoretical ϵ^2 extracted from dilepton spectra in comparison with experimental HADES ϵ^2 .

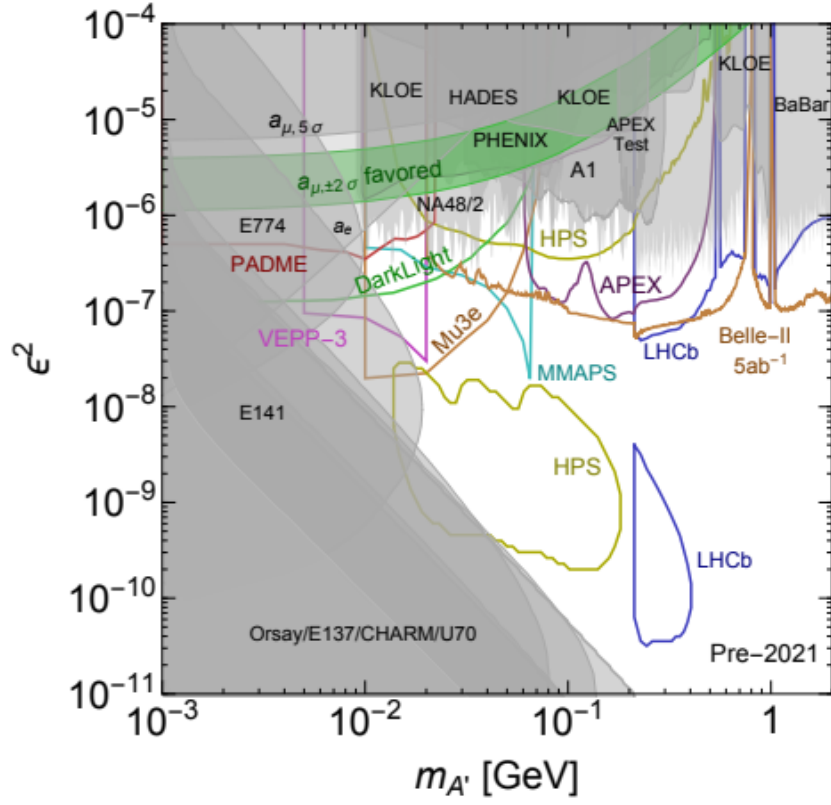


Figure 33: Constraints on ϵ^2 from other experiments. Figure is taken from [3].

Compared to other experiments, the found ϵ^2 from HADES and PHSD lie good within the expected ranges given by other experiments. As one can see on the right side of fig. 32, the constraints on ϵ^2 vs the mass are in the upper region of the obtained results from different experiments.

9 Conclusions

In this thesis, the interaction with SM matter of possible U-Boson decays to dilepton spectra from p+p and p+Nb collisions at 3.5 GeV and Ar+KCl collisions at 1.76 A GeV has been studied from a theoretical point of view. The theoretical description of U-Bosons via portals has been discussed.

The study has been done based on the microscopic off-shell transport PHSD approach. The U-Boson production by π^0 and η mesons and the Δ baryonic resonance has been implemented in the PHSD code, as well as the U-Boson decay to e^+e^- pairs.

The mass of a U-Boson and its mixing parameter ϵ^2 which describes the coupling strength to ordinary matter are still unknown. The mixing parameter has been extracted from theoretically calculated dilepton spectra for the whole mass range $M_U < 1 \text{ GeV}/c^2$ by assuming that additional contributions resulting from $U \rightarrow e^+e^-$ decays cannot exceed the dilepton yield from SM dilepton channels by more than 20%. Thereby, the results stay within an upper limit of the experimental error bars of measured dilepton spectra. We note that the PHSD approach describes the dilepton spectra from SM channels very well. The DM contributions for decays of π^0 , η and Δ are smaller than their SM counterparts, but clearly present. The decays of vector mesons were not included in these calculations, which causes a less accurate result for ϵ^2 at masses above 0.6 GeV.

From these, a theoretical upper limit for the coupling of U-Bosons to SM matter has been extracted. The theoretical results for ϵ^2 from p+p, p+Nb, and Ar+KCl spectra agree with the HADES results for ϵ^2 at $M_U = 0.2\text{-}0.4 \text{ GeV}/c$. At larger M_U they provide a lower upper limit for ϵ^2 . Experiments worldwide find comparable results, albeit most of them predict a lower upper limit.

Up to now, no peak structure on top of the spectra has been measured. All calculations and measurements are based on theory without proof. Nonetheless, the approach to find a Dark Photon is very promising and may one day be successful. The search for Dark Photons continues!

References

- [1] F. Zwicky. “The Coma Cluster of Galaxies”. In: 63.371 (Apr. 1951), p. 61. DOI: 10.1086/126318.
- [2] G. Bertone and D. Hooper. “History of dark matter”. In: *Rev. Mod. Phys.* 90.4 (2018), p. 045002. DOI: 10.1103/RevModPhys.90.045002. arXiv: 1605.04909 [astro-ph.CO].
- [3] J. Alexander et al. “Dark Sectors 2016 Workshop: Community Report”. In: Aug. 2016. arXiv: 1608.08632 [hep-ph].
- [4] Vera C. Rubin, Jr. Ford W. Kent, and Norbert Thonnard. “Extended rotation curves of high-luminosity spiral galaxies. IV. Systematic dynamical properties, Sa through Sc”. In: *Astrophys. J. Lett.* 225 (1978), pp. L107–L111. DOI: 10.1086/182804.
- [5] *Galaxy rotation curve*. URL: https://en.wikipedia.org/wiki/Galaxy%5C_rotation%5C_curve. (accessed: 09.01.2021).
- [6] *NASA Finds Direct Proof of Dark Matter*. URL: https://chandra.harvard.edu/press/06%5C_releases/press%5C_082106.html. (accessed: 09.01.2021).
- [7] Alan G. Aversa. *Modified Newtonian Dynamics (MOND) and the Bullet Cluster*. URL: http://www.u.arizona.edu/~aversa/aversa_400b_paper.pdf. (accessed: 10.01.2021).
- [8] “WIMPs and MACHOs”. In: *Encyclopedia of Astronomy and Astrophysics* (). URL: <https://sites.astro.caltech.edu/~george/ay20/ea-wimps-machos.pdf>.
- [9] D. Tovey C. Doglioni. *Searching for Dark Matter with the ATLAS detector*. URL: <https://atlas.cern/updates/feature/dark-matter>. (accessed: 09.01.2021).
- [10] D. Bauer et al. “Dark Matter in the Coming Decade: Complementary Paths to Discovery and Beyond”. In: *Phys. Dark Univ.* 7-8 (2015), pp. 16–23. DOI: 10.1016/j.dark.2015.04.001. arXiv: 1305.1605 [hep-ph].
- [11] G. Bertone, D. Hooper, and J. Silk. “Particle dark matter: Evidence, candidates and constraints”. In: *Phys. Rept.* 405 (2005), pp. 279–390. DOI: 10.1016/j.physrep.2004.08.031. arXiv: hep-ph/0404175.
- [12] K. Freese, M. Lisanti, and C. Savage. “Colloquium: Annual modulation of dark matter”. In: *Rev. Mod. Phys.* 85 (2013), pp. 1561–1581. DOI: 10.1103/RevModPhys.85.1561. arXiv: 1209.3339 [astro-ph.CO].

- [13] *What is the Universe Made Of?* URL: https://wmap.gsfc.nasa.gov/universe/uni%5C_matter.html. (accessed: 09.01.2021).
- [14] *Standard Model*. URL: <https://www.physik.uzh.ch/en/researcharea/lhcb/outreach/StandardModel.html>. (accessed: 09.01.2021).
- [15] W. Cassing and E.L. Bratkovskaya. “Parton-Hadron-String Dynamics: an off-shell transport approach for relativistic energies”. In: *Nucl. Phys. A* 831 (2009), pp. 215–242. DOI: 10.1016/j.nuclphysa.2009.09.007. arXiv: 0907.5331 [nucl-th].
- [16] E.L. Bratkovskaya et al. “Parton-Hadron-String Dynamics at Relativistic Collider Energies”. In: *Nucl. Phys. A* 856 (2011), pp. 162–182. DOI: 10.1016/j.nuclphysa.2011.03.003. arXiv: 1101.5793 [nucl-th].
- [17] W. Ehehalt and W. Cassing. “Relativistic transport approach for nucleus nucleus collisions from SIS to SPS energies”. In: *Nucl. Phys. A* 602 (1996), pp. 449–486. DOI: 10.1016/0375-9474(96)00097-8.
- [18] W. Cassing and E.L. Bratkovskaya. “Hadronic and electromagnetic probes of hot and dense nuclear matter”. In: *Phys. Rept.* 308 (1999), pp. 65–233. DOI: 10.1016/S0370-1573(98)00028-3.
- [19] C. E. Detar et al. “String breaking in lattice quantum chromodynamics”. In: *Phys. Rev. D* 59 (1999), p. 031501. DOI: 10.1103/PhysRevD.59.031501. arXiv: hep-lat/9808028.
- [20] W. Cassing. “Dynamical quasiparticles properties and effective interactions in the sQGP”. In: *Nucl. Phys. A* 795 (2007), pp. 70–97. DOI: 10.1016/j.nuclphysa.2007.08.010. arXiv: 0707.3033 [nucl-th].
- [21] T. Kodama et al. “Causality and relativistic effects in intranuclear cascade calculations”. In: *Phys. Rev. C* 29 (1984), pp. 2146–2152. DOI: 10.1103/PhysRevC.29.2146.
- [22] K. Kajantie E. Byckling. *Particle Kinematics*. John Wiley & Sons, 1972.
- [23] C. A. Salgado. *Understanding the Physics of Heavy Ion Collisions*. URL: <http://blois.in2p3.fr/2011/transparencies/salgado.pdf>. (accessed: 09.01.2021).
- [24] M. Weber et al. “Inclusive e^+e^- pair production in $p + p$ and $p + \text{Nb}$ collisions at $E(\text{kin}) = 3.5\text{-GeV}$ ”. In: *J. Phys. Conf. Ser.* 316 (2011). Ed. by Rene Bellwied and Claude Pruneau, p. 012007. DOI: 10.1088/1742-6596/316/1/012007.
- [25] G. Agakishiev et al. “First measurement of proton-induced low-momentum dielectron radiation off cold nuclear matter”. In: *Phys. Lett. B* 715 (2012), pp. 304–309. DOI: 10.1016/j.physletb.2012.08.004. arXiv: 1205.1918 [nucl-ex].

- [26] G. Agakishiev et al. “Inclusive dielectron spectra in p+p collisions at 3.5 GeV”. In: *Eur. Phys. J. A* 48 (2012), p. 64. DOI: 10.1140/epja/i2012-12064-y. arXiv: 1112.3607 [nucl-ex].
- [27] G. Agakishiev et al. “Dielectron production in Ar+KCl collisions at 1.76A GeV”. In: *Phys. Rev. C* 84 (2011), p. 014902. DOI: 10.1103/PhysRevC.84.014902. arXiv: 1103.0876 [nucl-ex].
- [28] E.L. Bratkovskaya et al. “System size and energy dependence of dilepton production in heavy-ion collisions at 1-2 GeV/nucleon energies”. In: *Phys. Rev. C* 87 (2013), p. 064907. DOI: 10.1103/PhysRevC.87.064907. arXiv: 1301.0786 [nucl-th].
- [29] G. Agakishiev et al. “Searching a Dark Photon with HADES”. In: *Phys. Lett. B* 731 (2014), pp. 265–271. DOI: 10.1016/j.physletb.2014.02.035. arXiv: 1311.0216 [hep-ex].